12-2021

Characterization of Biomarkers for Alzheimer's Disease and HIV-1 Associated Neurocognitive Disorders

Armando Garces III
The University of Texas Rio Grande Valley

CHARACTERIZATION OF BIOMARKERS FOR ALZHEIMER'S DISEASE AND HIV-1 ASSOCIATED NEUROCOGNITIVE DISORDERS.

A Thesis

by

ARMANDO GARCES III

Submitted in Partial Fulfillment of the

Requirements for the Degree of

MASTER OF SCIENCE

Major Subject: Biochemistry and Molecular Biology

The University of Texas Rio Grande Valley

December 2021

CHARACTERIZATION OF BIOMARKERS FOR ALZHEIMER'S DISEASE AND HIV-1 ASSOCIATED NEUROCOGNITIVE DISORDERS.

A Thesis
by
ARMANDO GARCES III

COMMITTEE MEMBERS

Dr. Upal Roy
Chair of Committee

Dr. Hansapani Rodrigo
Committee Member

Dr. Mario Gil
Committee Member

December 2021

ABSTRACT

Garces III, Armando, Characterization of Biomarkers for Alzheimer's Disease and HIV-1 Associated Neurocognitive Disorders. Master of Science (MS), December, 2021, 101 pp., 6 tables, 20 figures, references, 113 titles.

Alzheimer's disease is a neurodegenerative disorder that is characterized by progressive cognitive decline and the accumulation of amyloid beta and neurofibrillary tangles in regions of the brain. These protein deposits are known to generate multiple effects on the brain that lead to neurodegeneration. It has been established that (Human Immunodeficiency Virus) HIV-1 accelerates the aging process of people living with HIV-1. Moreover, there is significant clinical evidence indicating a potential link between the neurodegeneration developed by those with an HIV-1 infection and AD. HIV-1 viral infection causes cognitive impairment known as HIV-associated neurocognitive disorders. Most of the underlying mechanism between HAND and AD is not well characterized. This study explores the possibility of identifying common differentially expressed genes, that may serve as biomarkers for early detection or intervention Transcriptome profiles of both pathologies will be used in order to identify biomarkers that will be further explored using Alzheimer's disease models.

DEDICATION

I want to dedicate the completion of my master's studies to my family, who have supported me throughout my academic career. Especially both of my grandparents Armando Garces Garces and Juanita Miller, who suffered from Alzheimer's disease. They gave me purpose to pursue a solution for this health crisis we are currently facing. My mother Elvia Alicia Quintero Garces, my father Armando Garces, my sister Elvia Amparo Garces Quintero, and my brother Brandon Garces. I would also like to dedicate this to my extended family and friends.

ACKNOWLEDGMENTS

I want to thank Dr. Upal Roy for allowing me to work alongside him. His mentoring and ideas allowed me to grow as a professional student and allowed my confidence to grow. Mrs. Deepa Roy for making sure I had everything I needed so projects would go as planned and the rest of the team Caroline, Joe, and Natalia. Special thanks to my committee members. Dr. Rodrigo for training me on using various statistical tools that were a key component for this study. I also want to thank Dr. Mario Gil for his expert advice and guidance throughout this study. I would also like to acknowledge Dr. Zaire, who played an instrumental part in protein detection in our analysis. Also, Dr. Fields and his team for their contribution in reviewing the material. I want to thank the College of Sciences and the Office for Sustainability from the University of Texas Rio Grande Valley for their opportunity to continue my path as a professional student. I would also like to acknowledge the Serafy Endowment of Brownsville and the NIH grants: NIH/NINDS (R15NS108815) and NIH/NIAID (R01AI147731) for financial support for this study.

I would also like to acknowledge my parents Armando Garces and Elvia Alicia Garces Quintero, who have dedicated their time and effort to the position I am in right now. I would also like to acknowledge my siblings Elvia Amparo Garces Quintero and Brandon Garces for always being there for me when I needed them the most.

TABLE OF CONTENTS

Page

LIST OF TABLES

Page

LIST OF FIGURES

Page

CHAPTER I

ALZHEIMER'S DISEASE IN AGING POPULATION

Statement of Problem

According to the Alzheimer's Association, Alzheimer's disease (AD) is the most common form of dementia in the United States. In 2020, approximately 5.8 million people over 65 lived with AD in the United States (Alzheimer's Association, 2020). Age is a significant risk factor for AD—the likelihood of developing AD doubles every five years after the age of 65. The age individuals are affected by AD characterizes two forms of AD, known as early-onset AD and late-onset AD. Being diagnosed at a later age is generally known as late-onset AD and is responsible for 96% of all cases (Canet et al., 2018). Early-onset accounts for about 4% of AD patients, and it is a very rare form of the disease which affects patients at an earlier age between 30 to 60 years. Dr. Alois Alzheimer first observed the disease through histopathological observations of the brain of a deceased patient admitted for care due to progressive cognitive decline. His publishing in 1907 was the first to link senile plaques and neurofibrillary tangles with dementia (Hippius & Neundörfer, 2003).

Since discovering the disease, AD has been a great challenge for scientists due to its multifactorial pathology. An exact molecular mechanism for AD development has not been established (Bilousova et al., 2020). However, many studies have focused on the two hallmarks

The accumulation of extracellular amyloid-beta (Aβ) protein forms senile plaques and neurofibrillary tangles due to intracellular hyperphosphorylated tau proteins (Battacharya, 2015; Ferreira et al., 2016; Riphagen et al., 2020; Yoon & Kim, 2016). Cholinesterase inhibitors are one of the main options for treating neurodegenerative diseases like AD, Parkinson's disease, and Lewy body dementia (Bhattacharya et al., 2015; Colovic et al., 2013; Jin et al., 2021). The first approved cholinesterase inhibitor for treatment in the US was Tacrine in 1993 was prohibited due to its toxicity (Colovic et al.,2013). Currently, there are three FDA-approved cholinesterase inhibitors in the US used for mild to moderate AD treatment (Colovic et al., 2013). These FDA-approved drugs are donepezil, rivastigmine, and galantamine (Okello & Mather,2020). They reduce cognitive symptoms essential for daily interactions like memory, language, and judgment (Colovic et al., 2013; Jin et al., 2021). Even though they are an essential option for treatment, they cannot reverse or stop AD.

The Socioeconomic Burden for the Latino/Hispanic Population

The Centers for Disease Control and Prevention (CDC) estimates that the Latino population over 65 will quadruple, increasing the number of Latinos affected by AD in the US to 3.5 million. The Hispanic population is expected to increase by over 20 million in Texas by 2050. Age is a significant risk factor for AD, and the RGV has a higher life expectancy than other Texas regions (Valencia, 2019). Generally, as the population reaches the age of 65, the risk of developing the disease doubles every five years (Isik, 2010). Studies show that the Latino population has a younger onset age and is 1.5 times more likely to develop AD than the white non-Hispanic population (Vega et al., 2017). In the United States, 12% of the adults in Hispanic people are diagnosed with AD making it the highest percentage among other racial groups (Vega

et al., 2017). The Latino community is predisposed to diseases that may increase the risk of developing AD. Some of these diseases include cardiovascular disease and are 64% more likely to develop diabetes than the white non-Hispanic population (Alzheimer's Association, 2020). The Rio Grande Valley (RGV), located in South Texas, is primarily Hispanic. In 2017, the Hispanic population in counties that make up the Rio Grande Valley (RGV) ranged from 71-99% (Valencia, 2019).

AD has had a tremendous socioeconomic burden on the community as the aging population increases; the cost is estimated to reach 1 trillion in the US by 2050 (Alzheimer's Association, 2020). The high cost of treatment and disease-related cost makes it difficult to provide the proper treatment and assistance needed. The Hispanic community has higher rates of poverty when compared to non-Hispanic whites (Sheffield & Peek, 2009). According to Alzheimer's Association, education can have protective effects against AD. Studies show that a high level of education, socioeconomic status, and cognitive leisure activities promote cognitive reserve and are considered independent protective factors against mild cognitive impairment and AD (Jefferson et al., 2011; Sattler et al., 2012). However, one in 10 Hispanic elders have no formal education and have the lowest percentage of education received in Texas (Jefferson et al., 2011; Sattler et al., 2012). Latinos living in low-income neighborhoods associated with education levels are three times more likely to develop cognitive impairment (Vega et al., 2017). In the Rio Grande Valley, the population is predominately Hispanic, and considering the average annual income of the Rio Grande Valley is $50,000, the community is at a disadvantage to access these types of resources (Valencia, 2019). It is vital to continue to understand the complex pathology of AD to develop effective measures to slow or stop the progression of AD. For

researchers to create therapeutic drugs, it is crucial to understand the regulation of genes in the brain to identify a potential target further to investigate AD pathology.

Statement of Purpose

Identifying Common Biomarkers in Neurodegenerative Disease

AD has become a growing concern among people over the age of 65 as medical science advances our life expectancy. The multifactorial pathology of AD that affects the central nervous system has been observed in other diseases, including Human Immunodeficiency Virus -1 (HIV-1) infection (Kodidela et al., 1992; Milanini et al., 2019; Pulliam et al., 2019). HIV-1 infection may accelerate the brains' aging process, leading to HIV-associated neurocognitive disorders (Solomon et al., 2017). Significant clinical evidence indicates a potential link between the neurodegeneration developed during HAND and AD. However, the relationship between HAND and AD is still not well characterized (Kahn et al., 2019; Rubin et al., 2019; Solomon et al., 2017). Therefore, the current study investigated an *in situ* genome-wide screening of transcription regulators in brain tissue, identifying genes that can be used as biomarkers for early detection.

According to the United Nations AIDS (UNAIDS) organization, in 2020, 37.7 million people were living with HIV-1 worldwide, and 1.2 million of these patients were in the United States (Hairiri & Mckenna, 2007; Rubin et al., 2019; UNAIDS, 2021). Even though combination antiretroviral therapy (cART) has successfully suppressed viral loads, HAND affects as high as 50% of HIV-1 patients treated with cART. This may be due to the brain's role as a reservoir for HIV-1, where the virus enters the brain early during infection and has been detected in the white matter of postmortem brain tissues. Many studies have focused on investigating brain tissue

samples to identify the critical pathophysiological features of patients with different severity levels of HAND (Rumbaugh & Tyor, 2015). Interferon response genes (IFRG), which are related to the cell functions in the immune system and autoimmunity, were differentially expressed in the brain of HAND subjects (Everall et al., 2005; Gelman et al.,2012; Masliah et al., 2004). In HIV-1 infection, the virus enters the brain early after infection, where it begins replicating within the microglia and perivascular macrophages, eventually causing neuronal damage that promotes the onset of the symptoms associated with HAND (Garcia-Mesa et al., 2016). A recent study has found that the symptoms observed in HAND patients have developed into AD-like symptoms (Kahn et al., 2019). The compounding effects of HIV-1 and its influence on aging for those with the virus urge further investigation to determine the pathology of AD and HAND among PWH to improve prognosis and treatment outcomes (Rubin et al., 2019). Therefore, developing a set of biomarkers that can differentiate and detect AD and HAND in aging individuals with HIV-1 (Rosenthal & Tyor, 2019).

The accumulation of extracellular Aβ protein and intracellular hyperphosphorylated tau protein in various brain regions has been the disease's two main hallmarks since they were identified more than 100 years ago (Hippius & Neundörfer, 2003). In addition, comparative studies indicate that amyloid plaques were observed in HAND patients, suggesting that HAND may lead to AD (Fulop et al., 2019; Howdle et al., 2020). Similarly, studies demonstrate that combination Antiretroviral Therapy (cART) treatment is associated with increased Aβ levels in the cerebral spinal fluid (CSF) of people with asymptomatic neurocognitive disorders (ANI) and decreased levels in individuals with HIV-associated dementia (HAD) (Fields et al., 2020). While this data suggests that Aβ clearance varies between HAND groups, the relationship between Aβ levels in CSF and cognitive impairment deserves further investigation (Fields et al.,2020).

Triggering receptor expressed on myeloid (TREM) 2 has been associated with AD and has various functions, including regulating neuroinflammation and the clearance of Aβ (Fields et al., 2018). Brain protein levels and cellular localization of TREM2 were found altered in people with HIV-1 (PWH) with HAND, suggesting a common pathogenic mechanism in the two neurodegenerative diseases (Fields et al., 2018). The interaction of Aβ in people infected with HIV-1 can disrupt various processes that may lead to AD, including the development of neurodegeneration.

People with HIV-1 experience premature aging and an increased risk of age-related complications. HIV-1 infection may lead to neurodegeneration and cause AD-like symptoms; therefore, differentiating between these diseases has become an issue (Kodidela et al., 2019). However, in HIV-1 patients, intracellular Aβ deposits have been identified and are suggested to be involved with neuronal damage due to the cells' inability to clear these deposits (Achim et al., 2009; Green et al., 2005). An Aβ deposition was identified in the frontal lobe regions and mid-temporal regions in PWH (Esiri et al., 1998; Rubin et al., 2019). A study using neuroimaging and neuropsychological profiles identified abnormalities in the brains of MCI-AD and HAND. Researchers reported distinct atrophy patterns in the brains of people with AD and HAND (Milanini et al., 2019). We suggest that comparing the differentially expressed genes through genome-wide association studies (GWAS) of both AD and HAND patients will identify pathways that may be involved in the neurodegeneration of these diseases (Figure 1).

This study focused on identifying common RNA co-expressed in AD and HAND pathologies using linear regression models and more robust significance analysis of microarray (SAM). Transcriptome profiles were gathered from post-mortem brains of people with AD and

HAND and compared to identify common genes whose expression is dysregulated and could serve as biomarkers for future studies. Identifying biomarkers of neurological diseases can help determine the critical pathways involved in neurodegeneration. Gene functional analysis was performed to help identify the functions of various gene clusters to help distinguish which pathways are affected. This information will contribute to the identification of potential biomarkers that can detect the early neurodegeneration common in the aging population of people with HIV-1. Overall, the findings in this study implicate the dysregulation of STAT1, IFIT3, ISG15, and GBP1 genes associated with pathways in the human brain that may directly or indirectly regulate AD pathology in people with HIV-1. Further investigation will be needed to confirm these observations using in vitro AD models to understand better which biomarkers may be involved in the neuropathology of AD.

Aβ Induced Immune Response in AD

AD is a multifactorial disease with many factors that contribute to the development of the disease over time. The gene and environment interaction over time can contribute to the development of the disease. Over time, the gene and environment interaction includes many factors that may be difficult to quantify. However, we can identify which genes are affected by recreating the environment using in vitro models. Throughout the brain regions, senile plaques form due to the accumulation of Aβ protein deposits. The accumulation results from pathological cleavage of the amyloid precursor protein (APP) by ß-secretase, which results in a C99 fragment; a subsequent cleavage by gamma-secretase produces the insoluble Aβ (De Strooper & Annaert, 2000; Soontornniyomkij, 2019). Aβ is one of the two hallmarks seen in AD Aβ can initiate various signaling cascades, including caspase activation, lipid peroxidation, and DNA damage

associated with neuronal cell death. Cells have a defense mechanism that is activated through amyloid precursor processing (Li et al., 2019). A study establishing an AD model representing AD in the early stages demonstrates that acute high doses produced significant functional impairment and increased cell death. In contrast, low chronic doses had functional impairment without affecting the cell viability. The study suggests that low chronic dosages are better to represent the early stages of AD (Berry et al., 2018). High levels of cell death in neuronal cells due to Aβ treatment represent the late stages of AD. Studying this treatment is not ideal due to the damage done to neuronal cells that may be irreversible (Berry et al.,2018; DeKosky & Scheff, 1990). Replicating this in our study is important because our samples are from definite AD at the time of death. Assuming there was already significant cell damage and death for the analysis, we are interested in this chronic exposure model for high cell death levels.

The type 1 interferon pathway is a signaling cascade triggered in response to viral or bacterial infection. Type 1 interferons are cytokines whose purpose is to protect uninfected cells from disease. All the host's cells can secrete interferons when they recognize viral proteins. Once the IFN is secreted, they bind to a receptor known as IFNAR, which can interact with IFN-α/ß all the Type 1 interferon subtypes. Once it binds with the IFNAR receptor, it activates the ISGF3 transcription factor, consisting of STAT1, STAT2, and IRF-9, which are translocated into the nucleus and bind to the ISRE of the IFIT promoters. It has been observed that acute exposure to Aβ promotes the expression of protein inhibitor of activated STAT 1 (PIAS1). This inhibitor interferes with the binding affinity of STAT1, preventing the activation of downstream interferon-stimulated genes (Liu et al., 2019). There are multiple interferon-stimulated genes whose transcription is activated downstream of the JAK-STAT pathway.

IFIT3 is a gene that is dysregulated in AD, it has been observed that the expression of *IFIT* genes varies in different regions of the brain. The IFIT protein family, which includes IFIT3, is found in the cytoplasm. They are made up of multiple tetratricopeptide repeats consisting of 34-amino-acid helix turn helix motifs. IFIT3 has been observed to be expressed in cerebellar granule cells (Fensterl & Sen, 2015). This gene has also been observed in other neurodegenerative diseases. A study on HIV neuro aids shows a dysregulation of *IFIT3*, *MX1*, and *STAT1* (Winkler et al., 2012). This gene can also go by *ISG60* and has been associated with anti-proliferative and anti-viral functions. Many of its biological functions still need to be determined. *IFIT3* is induced through IFN-ß and has been observed to regulate the expression of chemokine *CXCL10*. They report that IFN-ß has a positive feedback loop with P-STAT1. This means that the expression of *IFIT3* can promote P-STAT1 activation of itself and other IFN stimulated genes (Imaizumi et al., 2016). It has also been observed that upon removal of *IFIT3*, increased levels of cell death are observed (Hsu et al., 2013; Sasaki et al., 2021). We must understand how this gene is regulated in distinct regions of the brain because it has been suggested to have detrimental effects when it is both upregulated and downregulated.

In vitro studies of the IFIT3 expression in a neuronal cell following Aβ treatment have not been published. Therefore, investigating how the expression of IFIT3 based on Aβ treatment in vitro may give us an idea of how IFIT3 is regulated during AD development. Essentially, they can serve as markers that can be measured in individuals exposed to detect the disease at an early stage in which intervention can be more affected. These biomarkers may serve as a target for future drug development. Our genome-wide analysis results have highlighted some pathways involved in the immune response. The immune response releases proinflammatory cytokines,

which trigger inflammation from special cells responsible for maintaining balance in our CNS and has recently gained more attention due to supporting data.

Objectives and Hypothesis

The specific objective of this study is to identify common genes that are dysregulated in both AD and HAND to understand further which pathways are involved in the neurodegeneration seen in AD. The study will be approached using two separate specific aims. The first specific aim consists of genome-wide association studies (GWAS) of post mortem brain samples derived from AD and HAND patients. These datasets will be extracted from National Center for Biotechnology Information (NCBI) GEO omnibus will be analyzed using statistical analyses, including significance analysis of microarray and linear regression models to identify differentially expressed genes (DEGs) by comparing AD and HAND to healthy controls. To further investigate the observations made from post mortem brain samples, we will develop an in vitro model of AD using Aβ (25-35). We will then further characterize IFIT3 and STAT1 by measuring cell protein and mRNA levels. We hypothesize that STAT1 and downstream gene IFIT3 will be downregulated in AD in vitro and ex vivo models.

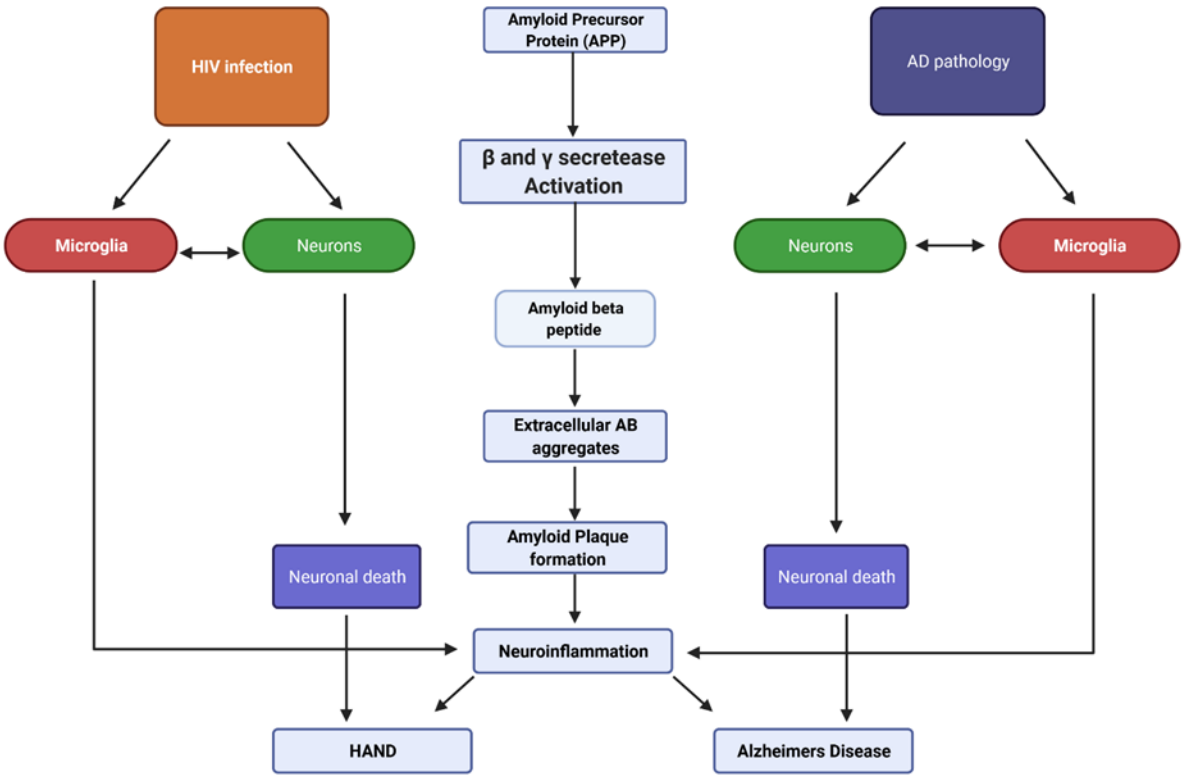

Figure 1: Neurodegenerative pathway in HAND and AD. This figure represents the overlapping pathology involved in the neurodegeneration of both AD and HAND. Both pathologies share similar neuronal death and neuroinflammation that leads to either HAND or AD. Further investigation on the transcriptome profiles of patients with AD and HAND by comparing them to healthy controls will allow the identification of common pathways involved in the neurodegeneration of these diseases.

CHAPTER II

METHODOLOGY AND FINDINGS

Methodology for Aim 1: Datasets and Subjects

This study investigated three different transcriptome profiles containing either HAND or AD-derived patient data. The mRNA-based datasets were obtained from the Gene Expression Omnibus (GEO) database that is maintained by the National Center for Biotechnology Information (NCBI) (Clough et al.,2016). The ages of subjects in the dataset GSE28160, which contains HAND data, ranged from 21 to 64 years with a mean age of 46. The AD dataset was found using accession number GSE84422 and contains three platforms described in this research that were categorized based on the Affymetrix chip used to collect data. The age of subjects in the dataset GPL 570 ranged from 62 to 102 years, with a mean age of 87. The ages of AD subjects in two GEO platforms (GPL), GPL96 and GPL 97, ranged from 60 to 100 years with a mean age of 86. The data contained in GPL 96 and GPL97 were averaged based on the original publication (Sun et al., 2019). Both GPL 96 and GPL97 contained 48 White subjects, 12 Black, 2 Hispanic, and 1 Asian subject, with 41 females and 22 males. In GPL 570, there were 42 female subjects and nine male subjects. Although the subject list was diverse, it was mainly White with 36 subjects, while 11 were Black, 2 Hispanic, and 1 was Asian Gene expression data were normalized GCRMA adjusts for background intensities in Affymetrix array data, including

optical noise and non-specific binding (Wu & Irizarry, 2021).

Principal Component and Linear Model Analyses

Principal component analysis was used to visualize subjects' gene profiles in low dimensional space and investigate the presence of any clustering effect among subjects within the same disease group in each data set. Further analyses were performed with Linear models and Significance Analysis of Microarrays (SAM). These approaches helped identify differentially expressed genes with non-normal distributions and whether the variability of these expression values differs between genes. Filtered log2 gene expression data was utilized to fit linear models for each brain region consisting of the basal ganglia and frontal cortex regions from the GSE84422 dataset and white matter regions from the GSE 28160. The amygdala and nucleus regions were also analyzed but were found only in the AD dataset. This method used weighted least squares with empirical Bayes moderation of the standard errors (Smyth, 2004). The limma Bioconductor package was used to manipulate the data to generate a list of differentially expressed genes.

Significance Analysis of Microarrays (SAM)

SAM is a popular nonparametric method that can be used to identify DEGs among different subject groups (Tusher et al.,2001). DE genes can be identified after controlling for false discovery rates in large and small samples (Chu et al., 2005). SAM helps to identify expression patterns that have slight yet significant differences between the control and other subject groups. This robust test has the advantage over the regular t-test as it applies even when the samples are neither independent nor normally distributed. The "samr" package in R (version

3.6.1) was used to perform the SAM analysis and report the SAM score (d), fold change, and the q-value of each gene. The q-value of a gene represents the false discovery rate of the gene list and includes that gene along with all other more significant genes 31. It is similar to the well-known "p-value," except it is adjusted so that many genes can be analyzed to determine the significance of a specific observation. The q-value measures how significant the gene is: as $d > 0$ increases, the corresponding q-value decreases. Differentially expressed genes with at least a two-fold change were identified within a 10% false discovery rate in all SAM analyses. This data was used to make a pairwise comparison between AD and Control, untreated HAND and Control, and cART treated HAND and Control, with the corresponding normalized data.

Gene ontology & Pathway Analyses

Gene Ontology and pathway analyses help identify the biological, molecular, and cellular functions of the common DE genes among the AD and HAND subjects. In this regard, the genes with a q-value of zero from the SAM analysis were used to compose the list of common genes. The list of common genes was analyzed using the official Affymetrix gene symbols using the "Functional Annotation Tool" found on DAVID (Huang et al., 2009). This analysis provided information on which pathways or processes are affected in both pathologies, allowing for further exploration of the function of specific genes.

Methodology for Aim 2: Developing AD *in vitro* Model

Cell Lines

The neuroblastoma cells (SH-SY5Y) (ATCC, Catalog # CRL-2266) were grown in a T-75 flask using EMEM media containing 10% Fetal Bovine serum. The experimental design is based on previous experiments on SH-SY5Y cell lines (Fang & Liu, 2008; Hashimoto et al., 2011; Lattanzio et al.,2016; Li et al.,2019; Wang et al., 2019; Yu et al., 2014).

Aβ Stock Preparation

SH-SY5Y Cells were treated with Aβ (25-35) peptides that were purchased from Sigma-Aldrich (Sigma Aldrich, Catalog # 173993-86-7) (Hashimito et al., 2011). The Aβ (25-35) is a peptide fragment that forms aggregates more efficiently than the full-length Aβ (1-42). It possesses the same biological properties as toxicity, so it is often used for in vitro drug studies (Yu et al., 2014). The stock solution of Aβ was used for treatment by diluting Aβ (25-35) into a 1mM working solution using autoclaved distilled water. In order to avoid thawing cycles, the 1mM stock solution was made by diluting 1mg of Aβ (25-35) in 1ml of autoclaved distilled water. The stock solution was incubated for seven days at 37°C with constant agitation to promote aggregation (Solomon et al., 1997). After the incubation, the stock solution was stored at –20 °C until use (Zhang et al., 2019). The concentration of 10µM, 20µM 60 µM Aβ (25-35) were optimized based on previous studies that resulted in apoptosis of SH-SY5Y neuroblastoma cells (Lattanzio et al., 2016; Li et al., 2019; Yu et al., 2014). Previous studies have shown that differentiated SH-SY5Y cells serve as clinically relevant cells in mature adults due to the post-mitotic characteristic. Cells required EMEM media containing 2mM glutamine with 50 ml of

FBS to create 10% FBS EMEM media used for regular culturing of SH-SY5Y cells. The cells were cultured when they reached 80% confluency. The media of the cells was replaced 24 hours after seeding with working media containing Aβ (25-35) stock solution for treatment supplemented with 2% FBS serum. The working solutions were made individually based on concentration. To determine the optimized concentration of other brain cells, we used Human microglial clone 3 (HMC3), which was cultured using 10% FBS EMEM and Human Astrocytes (HA) cultured using Astrocyte media, as they are all cells found in the Central Nervous System (CNS).

SH-SY5Y Cell Differentiation

Differentiation of SH-SY5Y was induced by replacing the media to culture cells with DMEM/F12 supplemented with 10% FBS with amphotericin B (Thermo Fisher Scientific, Catalog # 15290018) and gentamicin (MP Biomedical, Catalog # 1676045). Cells were grown until 80% confluency was reached and then subcultured based on the desired experiment. After 24 hours of incubation, media was replaced with 1% FBS DMEM/F12 media containing 10μM of all-trans-retinoic acid (ATRA). The media was changed every three days from the initial addition. Cells were treated on day 7 of differentiation for 96 hours incubated at 37C with 5% CO2.

Cytotoxicity of Aβ (25-35) on SH-SY5Y

Cytotoxicity (MTS) assay was utilized to observe the cell viability of SH-SY5Y after treatment of Aβ (25-35) with CellTiter 96® AQueous One Solution Reagent (Promega, Catalog # G3580). MTS assay was performed on 96 well plates (Thermo Fisher Scientific, Catalog # 07-

200-720A) using a 96-well plate reader (Biotek, Synergy HTX). SH-SY5Y cells were cultured as described above. Undifferentiated SH-SY5Y cells were plated in a 96-well plate at 80,000 cells per well, incubated for 24 hours. Differentiated cells were seeded at five $x10^4$ cells and treated on day seven. The Aβ (25-35) in three concentrations were prepared using the stock 1mM solution. A total of 1mg was needed to make 1mL of 1mM stock solution and was diluted with autoclaved deionized water. This stock is used to make the following concentrations in culture media in separate tubes of different concentrations.

Once concentration was made, 100µL were added from respective concentrations of Aβ (25-35) to the cells, and the plate was incubated for 24, 96 hours. On the day of the MTS assay, CellTiter 96® AQueous One Solution Reagent was taken out from -20°C and kept at room temperature to bring the temperature closer to 25°C (incubation in the dry bath or water bath is not recommended). The cells were washed with 100 µL of PBS. 100 µL of culture media was added to the wells. 20µL of CellTiter 96® AQueous One Solution Reagent was added into each well of the 96-well assay plate containing the samples in 100µl of culture medium. This is followed by incubating the plate at 37°C for 1 hour in a humidified, 5% CO2 atmosphere. After the incubation, the absorbance at record 490nm using the (Biotek, Synergy HTX) plate reader at 1hr and 4hr of incubation. Data were interpreted using absorbance using the following formula ((Sample/Control) x 100).

Flow cytometry and Permeabilized Labeling

Flow cytometry was done with differentiated and undifferentiated SH-SY5Y cells. Experimentally, cells were grown up to 80% confluency using complete (EMEM+10% FBS) media.

After incubation, 3.5. x10 ^{6} cells were treated with 10µM, 20µM, and 60µM of Aβ using 2% FBS supplemented EMEM for 96 hours. After incubation, cells were treated with the Trypsin enzyme and harvested and suspended in complete EMEM media. The cells were trypsinized, fixed with 4% paraformaldehyde for 20minutes, and permeabilized using a solution containing 0.1% Triton X-100 (Sigma Aldrich). Nonspecific binding was blocked using 5% Donkey serum in PBS + 1% BSA for 30 minutes at room temperature (RT). Primary polyclonal (STAT1) and Monoclonal (IFIT3) were added and incubated for two hours at room temperature. Cells were washed and incubated for 1 hour with FITC-conjugated affinity-purified donkey anti-mouse and Alexa647anti-rabbit antibodies (Jackson ImmunoResearch Laboratories). Cells were rewashed and split into two groups. One set of cells were used exclusively for flow cytometry (BD Accuri C6). The other set was used for permeabilized labeling by mounting them on a coverslip using ProLong antifade with DAPI (Molecular Probes). Images were acquired by a laser scanning confocal microscope (Olympus). All conditions, including optical sectioning, number of sections, and exposures, were identical for a given set of experiments.

ROS Assay with DCFDA

Differentiated and undifferentiated cells were cultured in black (transparent bottom) 96 well plates (Thermo Fisher Scientific, catalog # 165305) at a concentration of 80,000cells/100µL for undifferentiated cells and 50,000/100µL for cells undergoing differentiation two days before ROS assay for undifferentiated cells. Before starting the assay, a negative control was made by preparing 1mM catalase. Media was aspirated from 96 well plates and replaced with 100 µL of PBS into wells except for the wells that served as a negative control in which PBS+ catalase media was added and incubated for 2 hours. The PBS was removed, and 100µl of 100µM DCF-

DA was diluted with PBS and added to the wells incubated for 1 hour. After incubation, the DCF-DA solution was removed, and cells were treated with 10µM, 20µM, and 60µM of Aβ, H2O2, and catalase in their respective wells. The plate was immediately placed in the Bio Tek plate reader (Biotek, Synergy HTX) to measure the ROS production through the fluorescent unit (RFU) every hour up to18 hours using 480/20 excitation 528/20 emission. The data was represented with RFU on the y-axis and different treatments of cells on the x-axis.

STAT1 and *IFIT3* Gene Expression in SH-SY5Y Cells through RT- PCR

To measure the *STAT1* and *IFIT3* gene expression, SH-SY5Y cells were exposed to Aβ. After incubation, a total RNA extraction was performed based on the Qiagen RNA extraction kit (Qiagen, Catalog # 74004). Briefly, RNA extraction was done from a frozen cell pellet using RNase-free pipette tips, add 600 µl of lysis buffer was prepared with 1% two mercaptoethanol once added to the pellet. It was vortexed until the pellet was dispersed entirely. 600µl of 70% ethanol was added to the cell, followed by homogenization. A fraction of the sample (700µl) was transferred into a spin cartridge, including precipitant. The tube was centrifuged at 8,000 x g for 60 seconds, and the flow-through was discarded in the waste container. RW1 (700µl) wash buffer one was added to the spin cartridge. Followed by centrifugation at 8000 x g for 60 seconds, and flow-through in the collection tube was discarded in the waste container. Following that, 500 µl RPE Wash Buffer II was diluted with ethanol was added to the spin cartridge. It was centrifuged at 8000 x g for 2 minutes, and flow-through was discarded in the waste container. This step was repeated; however, the container was centrifuged for 5 minutes. The flow-through was 40 µl of RNase-free water was added and centrifuged at 8000 x g for 60 seconds, and the flow-through kept contained extracted RNA.

Following RNA extraction, samples were estimated through the Biotek analyzer. An equal RNA concentration was added in each well of the 96 well PCR plates based on the RNA concentration. The volume of the sample was maintained by adding DEPC water. A PCR master mix was prepared according to the number of samples. PCR plate was designed with GAPDH as a housekeeping gene and no template control and no primer control. Once all the reagents were ready, a master mix with respective primer was added to each well. After adding the sample, the plate was covered with the plate using adhesivetape, and after brief centrifugation, the plate was placed in the plate holder of the RT-PCR instrument (Thermo Fisher Scientific, Quanstudio3). The setting for the Quanstudio3 instrument. The setting for the Quanstudio3 instrument was set to "Instrument type: Quantstudio3", "System Block type: 96-well 0.1-ml Block"," Experiment type: Comparative Ct (ΔΔCT)", "Chemistry: TaqMan Reagents"," Run mode: Standard". The methods tab, the settings were as follows: “Volume” should be set at 20µl, and “Cover temperature” will be at 105.0 °C. After PCR was done, ΔΔCT value was collected for individual gene expression. Then comparative gene expression analysis was done with GAPDH. Following that, a fold change analysis was done with control and different treatment conditions (10, 20, 60µM). The graphical representation was based on fold change gene expression compared to untreated control.

Findings Aim 1: Identifying Biomarkers for AD

Statistical Significance of Datasets using Linear Models and Principal Component Analysis

Tables 2 and 3 have details related to comparisons AD vs. control and untreated HAND vs. control, respectively. DEGs for the AD data the brain regions analyzed were the basal ganglia, frontal cortex, and basal ganglia, and only white matter in the untreated HAND subject

was identified using linear models. The upregulated genes among a subject group compared to the other group in Table 2-3 are denoted by a log-fold value that is larger or equal to "1", down-regulated genes are denoted by a log-fold that is less than "1" and genes with no difference are denoted by "0". All linear model comparisons were made with the healthy control contained in each data set. Only the genes with significant p-values were considered for further analysis.

The treated HAND patient data did not show any significant change in gene expression. However, the untreated HAND patient data generated a list of 480 differentially expressed genes (DEGs); some of the upregulated genes can be seen in Figure 2, including *ISG15, IFIT3, STAT1, GBP1, C3*. Figure 2 provides a visual representation of the difference in expression observed between treated and untreated HAND and control subjects. The Z score indicates the expression levels, and the chart colors highlight whether a gene was over or under-expressed. Some genes that were upregulated in untreated HAND compared to controls include *STAT1*, *ISG15*, and *C3AR1*.

The data contained in the three platforms that make up the AD dataset were analyzed independently from the HIV-1 dataset. Figure 3 represents data from the nucleus accumbens and amygdala brain regions of subjects from the AD dataset. The comparison of AD vs. Control from the platform GPL570 contained 2,985 significant genes. Some of the important transcripts that were downregulated in GPL570 were *C3, C3AR1, DDR2, TLR7,* and *ANXA1*. In Figure 4, the frontal region data contained in GPL 96 had 1,379 DEGs, consisting of *GBP1, IFIT3, ISG15, STAT1*, and *DIRAS*. Platform GPL97 contained 575 genes and consisted of *IFIT3, GBP1*, *GABRB3*, and *DCLK1*. Interestingly, *IFIT3* appeared to be downregulated regardless of the platform used. Neither of the basal ganglia regions contained significant DEGs. Figure 5

represents a heatmap showing the expression levels of the basal ganglia after normalization. When comparing AD vs. Control, the basal ganglia did not show a significant change in expression of *STAT1, ISG15*, and *IFIT3* compared to what was observed in the frontal cortex.

The HAND subject and the distribution of these subjects within each brain region corresponds to the top three principal components where black represents the control, and HAND is red. In the untreated HAND group (Figure 6), clustering was found among the control subjects and HIV-1 subjects. However, a few outliers whose expression varied from the rest of the group are between 0 and 0.2 of the PC2 axis, above 0.2 of PC3, and between 0.15 and 0.12 of PC1.

In Figure 7, the AD subject data is represented by red, and the control subjects are represented by black. The nucleus accumbens and amygdala (Figure 7A) showed a significant amount of clustering in the negative direction of the PC1 axis, where both control and AD groups seemed to cluster together within the same area on the axis. AD subject data, however, spread out more, and some were seen on the positive end of the PC1 axis, indicating more variability of the subject data. Both frontal cortex plots (Figure 7B-C) showed data clusters on opposite ends of the PC1 axis. However, they both contained subject data clustered together and showed some variability among control groups along the PC2 axis. Figure 7D and 7E represent the basal ganglia subject data from platforms GPL96 and GPL97. More variability was observed in the expression of genes among AD basal ganglia samples seen in Figure 7D. However, there were some clusters of the control that were seen spread throughout the PC1 axis. AD clusters were observed between -0.14 and -0.13 of the PC1 axis. Within the basal ganglia, GPL97 showed clusters on the positive end of the PC1 axis towards 0.135 and between 0 and -0.2 of the

negative end of the PC2 axis (Figure 7 E). These clusters demonstrated similar expression in AD subjects that were used for the analysis. The difference seen in RNA expression may be due to the different chips used to analyze the patient samples; this is because of the range of RNA the Affymetrix was probed with for the experiment.

Identification of DEGs through SAM Analysis

Table 4 and 5 contains DEGs identified through the SAM analysis. Since the other two data sets contained controls, the focus was to identify common DE expressed genes in AD and untreated HAND or treated HAND postmortem brain samples. The treated HAND patient data resulted in 25 upregulated and 19 downregulated genes compared to the healthy control. When comparing untreated HAND patients to the healthy control, 52 downregulated genes and 397 upregulated genes were identified. The AD data contained three platforms, including GPL 570, which generated 385 upregulated genes and 62 downregulated genes. Figure 8 represents a Venn diagram comparing the SAM results from untreated HAND and AD subjects. A total of 30 genes were commonly dysregulated, including *C3* ((untreated HAND) 6.894 score (d): 14.104 fold change, q: < .001) ((AD) 3.623 score (d): 1.971 fold change, q: < .001), *C3aR1* ((untreated HAND) 5.468 score (d): 4.018 fold change, q: < .001) ((AD) 4.400 score (d): 1.867 fold change, q:< .001), *TLR7*((untreated HAND) 4.345 score (d): 8.197 fold change, q: .001) ((AD) 3.756 score (d): 1.945 fold change, q: .001), and *DTNA*((untreated HAND) 5.468 score (d): 4.018 fold change, q: .001) ((AD) 4.850 score (d): 1.916 fold change, q: .001)**.** The platform GPL96 contained basal ganglia regions that generated 40 downregulated genes, while the frontal lobe regions generated 109 downregulated genes and 17 upregulated genes. The AD data found in GPL97 had no DEGs in the basal ganglia regions and only 88 downregulated genes in the frontal

lobe regions. The results from GPL96 and GPL97 were averaged and used to compare with HAND subject data. Due to the lack of data from other brain regions in one HAND dataset, Figure 9 only represents data from the frontal cortex and white matter. A total of 14 genes were found shared between untreated HAND and AD, including *IFIT3*((untreated HAND) *6.086 score (d)*: 10.542 fold change, q: < .001) ((AD) -*3.628 score (d)* : .580 fold change, q:< .001), *ISG15* ((untreated HAND) *6.491 score (d*): 11.531 fold change, q: < .001) ((AD) -*3.342 score (d)* : .611 fold change, q:< .001), and *GBP1* ((untreated HAND) *5.530 score (d*): 9.495 fold change, q: < .001) ((AD) -*3.352 score (d)* : .585 fold change, q:< .001). As illustrated in Figure 11, these genes had an opposite expression in HAND and AD patients compared to Controls. Figure 10 represents data derived from the basal ganglia in which eight common genes, including *STAT1* and *GBP1*, were found shared between untreated HAND and AD.

Interestingly, a total of 15 DEGs that were shared between treated and untreated HAND patients had an opposite expression that depended on treatment. For example, *C4orf3* ((untreated HAND) -4.696 score (d): 0.580 fold change, q: < .001) ((treated HAND) score (d): 2.020 fold change, q: < .001) was upregulated in treated HAND subjects but downregulated in untreated HAND patients. Only two genes, *STK32A* ((treated HAND) score (d): 1.965 fold change, q: .001) ((AD) 3.532 score (d): 1.554 fold change, q: < .001) and *CD24* ((treated HAND) score (d): .109 fold change, q: < .001) ((AD) 3.460 score (d): 2.081 fold change, q: < .05), were found to be common and differentially expressed between treated HAND and AD. They were upregulated and downregulated respectively in HAND treated patients, and both were upregulated in AD patient data. For this reason, our focus was aimed at the untreated HAND subject data. There were many more genes in common between untreated HAND and AD patient's data when

regions of the brains were not considered, with a total of 51 common genes found dysregulated compared to healthy controls. The independent SAM results indicated that a total of 37 genes were upregulated in untreated HAND. Out of these 37 genes in HAND, 27 genes were upregulated, and ten were downregulated in an AD patient's sample.

Details of the complete list of genes that were up and downregulated among different subject groups across three brain regions can be found in Table 6. Table 2 summarizes the results of the SAM analysis, specifically the genes that were common between both pathologies. Figure 11 shows a visual representation of the genes that were more frequently observed throughout comparisons along with their expression levels in AD or HAND subjects, including *ISG15, GBP1, STAT1, IFIT3, and TLR7*.

Processes of Common Genes ISG15, GBP1, IFIT3, PLSCR1, STAT1, TLR7 Involved in Both AD and HAND

The list of 51 common genes between AD and untreated HAND was submitted to DAVID. As a result, our list majorly contributed to a total of 10 processes. Figure 12 represents the following genes and their respective processes, including the defense response to the virus, interferon-gamma-mediated signaling pathway, type 1 interferon signaling pathway, response to IFN-ß, chemical synaptic transmission, signal transduction, positive regulation of vascular endothelial growth factor, inflammatory response, and regulation of complement activation. Out of the 51 genes, 6 of them, *ISG15, GBP1, IFIT3, PLSCR1, STAT1,* and *TLR7*, were part of the defense response of the virus. A total of 8 genes are involved in signal transduction, including *ANXA1, C3, DDR2, DTNA, GABRB3, ITRP2, NRXN1*. There were three genes involved in the

type I interferon signaling pathway, *ISG15, IFIT3,* and *STAT1*. From the list, *STAT1* and *PLSCR1* genes are involved in response to IFN-ß. Both *C3* and *C3AR1* are involved in the regulation of complement activation and vascular endothelial growth production. *DLGAP1, DTNA*, *NRXN1,* and *SNAP25* genes are involved in chemical synaptic transmission. The inflammatory response genes from our list included *ANXA1, C3, C3AR,* and *TLR7*. The final process that our gene list was involved in was the regulation of bone mineralization which includes *BMP2K* and *DDR2*. The genes that were more frequently involved were *STAT1, C3,* and *C3AR1*

Pathway Analysis Identifies Key Pathways Involving CD44, FCGR1B, GBP1, and STAT1 Commonly Found in AD and HAND Datasets.

The list of common genes was submitted to DAVID, which generated three different REACTOME pathways. One of the REACTOME pathways was the interferon-gamma signaling pathway, which contained the genes *CD44, FCGR1B, GBP1,* and *STAT1*. The IFN-α/ß signaling pathway was the second pathway, which contained *ISG15, IFIT3,* and *STAT1*. The final pathway was the regulation of the complement cascade which included *C3* and *C3AR1*. For more details of genes and the processes they are involved in, please refer to Table 6.

Aim 2: Type 1 Interferon Signaling in AD model

Cell viability of SH-SY5Y Treated with Different Concentrations of Aβ

Exposing cells to Aβ at concentrations of 10μM, 20μM, and 60μM in undifferentiated SH-SY5Y did not show a significant reduction in cell viability at 24 hours of Aβ ($p=0.7159$). However, at 96 hours of treatment, results analyzed through a one-way ANOVA show that there

is a significant reduction in cell viability (F(3,20)=[4.396], p =0.0157). Dunnett's multiple comparison shows that the comparison between control vs 60μM has a significant mean difference (p=0.0435, 95% C.I.=[0.5453,42.16]) and no significant results were found in control vs 10μM (p=0.9946) and control vs 20μM (p=0.0797). A study comparing the cell viability of differentiated and undifferentiated showed that differentiated SH-SY5Y had a dose-dependent decrease of cell survival due to increasing Aβ concentration. Therefore, cells were differentiated using ATRA. The differentiated SH-SY5Y were treated for 24 hours, and one way, Anova reveals that there is a significant reduction in cell viability (F(3,20)=[7.08], p =0.0020). Dunnett's multiple comparisons found that the mean difference between control and 60μM was significant (p=0.0033, 95% C.I.=[4.661,23.97]), and there was no significant mean difference in control vs. 20μM (p=0.6842) and control vs. 60μM (p=0.9952). Similarly, after 96 hours of treatment, a one-way ANOVA reveals that there is a significant reduction in cell viability (F(3,18)=[5.547], p =0.0071). Dunnett's multiple comparison reveals no significant reduction in control vs. 10 (p=0.9591) and control vs. 20μM (p=0.0521). However, there was a significant reduction in 60μM treated differentiated SH-SY5Y (p=0.0065, 95% C.I.=[5.734,36.26]). To further confirm our effect of Aβ on other brain cells, HMC3 and HA were treated with the concentrations mentioned above of Aβ for 24 hours and 96 hours. Figure 13 shows a significant decrease in cell viability with 60μM Aβ treatment in all cells within 96 hours. The results of HA cells after 24-hour treatment were analyzed using one-way ANOVA, revealing that there is a significant mean difference to control (F(3,13)=[34.52], p =<0.0001). Following Dunnett's Multiple comparison showed a significant reduction for 60μM treated cells within 24 hours (p=<0.001, 95% C.I.=[15.87,35.42]) and no significant difference is observed in control vs

10μM (p=0.2283) and control vs 60μM (p=0.3019). At 96 hours, HA gradually declined cell viability with increasing concentrations of Aβ. A one-way ANOVA showed that there is a significant difference between control and treated cells (F(3,13)=[4.229], p =0.0272). Dunnett's multiple comparisons show that there is a significant mean difference between control vs. 60μM Aβ treated cells (p=0.0158, 95% C.I.=[10.56,99.53]), and no significant mean difference was found between control vs. 10μM (p=0.05939) and control vs. 20μM (p=0.0759). Since normality was not passed, data was analyzed using Kruskal Wallis analysis (H(2)=12.93, p=0.0001). Similarly, to undifferentiated cells HMC3 cells treated for 24 hours, a one-way ANOVA reveals no significant decrease in cell viability for any concentration (p=.7016). A one-way ANOVA analysis reveals that HMC3 resulted in a significant reduction in all treated cells (F(3,12)=[10.92], p =0.0084). Dunnett's multiple comparison shows that there is a significant mean difference in between control vs 10μM (p=0.0155, 95% C.I.=[4.461,41.16]), control vs 20μM (p=0.0042, 95% C.I.=[9.474,46.18]) and control vs 60μM (p=0.0004, 95% C.I.=[19.38,56.09]).

The Effect of Aβ on Reactive Oxygen Species (ROS) Generation in SH-SY5Y

In Figure 14, undifferentiated SH-SY5Y control cells produced more ROS than treated cells. A one-way ANOVA shows that there is a significant difference between catalase and control undifferentiated cells (F(3,12)=[10.93], p =<0.0001). Dunnett's multiple comparison confirms that the only significant difference in mean is control vs catalase (p=0.0046, 95% C.I.=[3256,21438]) and no significance is found between control vs H_20_2 and (p=.0871), control vs 10μM (p=0.0788), control vs 20μM (p=0.2963 and control vs 60μM (p=0.1895). Normality was not significant; therefore, data was analyzed through Kruskal Wallis analysis (H(4)=26.89,

p=<0.0001). However, one-way ANOVA shows that there is a significant mean difference between control and treated differentiated SH-SY5Y (F(5,44)=[8.646], p =<0.0001). Dunnett's multiple comparison revealed that there was a significant difference in ROS production between control and H_2O_2 (p=<0.0001, 95% C.I.=[-35272,11779]) and control vs 60µM (p=0.0124, 95% C.I.=[-21172,1990]). There was no significant ROS production between control and catalase ((p=0.999) control vs 10µM (p=0.9998) and control vs 20µM (p=0.9968).

IFIT3 and *STAT1* Transcripts in SH-SY5Y

Figure 15 RT-PCR was used to measure the *IFIT3* and *STAT1* gene expression in undifferentiated SH-SY5Y and differentiated SH-SY5Y after 96 hours of Aß treatment. The ct mean values were used to calculate each experimental variable's delta delta ct values. The delta-delta Ct values represent the fold change of each gene compared to *GAPDH* as the housekeeping gene. Two separate trials were ran for differentiated and undifferentiated SH-SY5Y cells. The values for each trial were used to calculate individual delta delta ct values. For the first trial of differentiated SH-SY5Y, the delta delta ct values of *STAT1* were 1 for control and 1.8025 for 10µM treated cells. At 20µM, the fold change increased to 2.24 and nearly doubled at 6.13 for cells treated with 60µM of Aß. The second trial for differentiated SH-SY5Y had 1 for control and had a fold change increase of 5.144 for 10µM treated cells. There is a reduction in fold change to 2.49 at cells treated with 20µM as the concentration increased to 60µM, a fold change increased to 3.51. In the first trial of differentiated SH-SY5Y, the delta delta ct values of *IFIT3* were 1 for control and .04753 for 10µM treated cells. At 20µM, the fold change increased to 1.79 and 3.60 in cells treated with 60µM of Aß, respectively. The second trial for differentiated SH-SY5Y had 1 for control and had a fold change increase of 7.006 for 10µM treated cells.

There is a reduction in fold change to 6.22 at cells treated with 20µM. As the concentration increased to 60µM, a significant fold change increased to 21.73. These results show an upregulation in mRNA of *IFIT3* and *STAT1* in differentiated SH-SY5Y after 96 hours of Aß treatment.

In the first trial of undifferentiated SH-SY5Y, the delta delta ct values of *STAT1* were similar in control and 10µM with a fold change of 1.07; however, there is a reduction 0.089 fold at 20µM and 0.84 fold with 60µM, respectively. The second trial for undifferentiated SH-SY5Y had 1 for control and had a reduction in fold change to 0.09 at 10µM treated cells and an increase to 0.40 with cells with 20µM. Cells treated with 60µM showed an increase in fold change to 2.72. For the first trial of undifferentiated SH-SY5Y, the delta delta ct values of *IFIT3* were was a 1.976-fold increase for 10µM treated cells. At 20µM, the fold change increased to 3.909 and was slightly reduced to 2.82 for cells treated with 60µM of Aß. The second trial for undifferentiated SH-SY5Y had 1 for control and had a fold change increase of .1415 for 10µM treated cells. Reduced *IFIT3* mRNA is seen in cells treated with 20µM with a fold change of .0505. However, as the concentration increased to 60µM, a fold change increased to 1.98. Even though the comparison of delta delta ct values between trials did not generate any significant results, our data show an upregulation of *IFIT3* and *STAT1* transcripts in Differentiated and Undifferentiated SH-SY5Y treated with 60µM of Aβ (25-35). The fold change was not used for statistical analysis because it cannot be normally distributed. Therefore, the delta CT values, which is the mean difference in expression between the gene of interest (*IFIT3* and *STAT1*) and the housekeeping gene (*GAPDH*) which can be normally distributed (Schmittgen & Livak, 2008). Figure 15 shows a heatmap representing the mean difference in *IFIT3* and *STAT1*, which

helps visualize the difference between groups. A one-way ANOVA analyzing the data from the undifferentiated SH-SY5Y cells shows no significant difference between treatment and control ($p=0.9709$). Similarly, differentiated SH-SY5Y cells did not show any significance ($p=0.9566$). This difference may be due to the high variance among the housekeeping gene *GAPDH*. Increasing the sample size to understand this variation in expression is currently in progress. Previous studies have had a similar issue in which RT-PCR data does not show significant results seen in array data (Liang et al., 2008).

IFIT3 and STAT1 Protein Expression in SH-SY5Y

In Figure 16, the results of two trials measuring the protein expression of STAT1 and IFIT3 in undifferentiated and differentiated SH-SY5Y cells after 96 hours of Aβ (25-35) treatment. These results did not generate significant results for STAT1 ($p=.2526$) and IFIT3 ($p=.3578$) in undifferentiated cells. Differentiated SH-SY5Y STAT1 and IFIT3 ($p=0.4029$) did not generate significant results either. However, there is a reduction in protein expression in cells treated with 60μM compared to 10μM and 20μM. The protein expression of cells treated with 20 μM of Aβ (25-35) had the highest translation rate. STAT1 protein levels are reduced compared to 20μM and 10μM, yet they are still higher than the control. For IFIT3 rate of translation is reduced to levels lower than the control for both differentiated and undifferentiated cells treated with 60μM of Aβ (25-35). Previous studies have reported a dysregulation in protein synthesis in different stages of the disease. They have reported an initial increase in the translational rate that is reduced over time (Ghosh et al., 2020). Increased cell death rates due to Aβ (25-35) toxicity represent late stages of AD, which is observed in cells treated with 60μM of Aβ (25-35). The cells treated with 10μM and 20μM have reduced cell death. However, there may still be

functional impairments; this is representative of the early stages of AD. In Figure 17, results for IFIT3 show an increase in protein expression in SH-SY5Y cells treated with 10μM and 20μM, which represent early stages and an increased translational rate supporting previous AD studies. Then there is a reduction in IFIT3 protein expression in cells treated with 60μM of Aβ (25-35). Future studies should measure IFIT3 protein to understand the gene expression in AD pathology further.

Table 1: Gene Expression Dataset Summary. This table describes the datasets used in this analysis. It specifically explains the pathology and the Affymetrix chips used to gather results and the number of subjects in each dataset. Abbreviations FC: Frontal Cortex, WM: White Matter, BG: Basal Ganglia, NA/AM: Nucleus Accumbens/Amygdala

Data Set ID	Pathology (HAND/ AD)	Database (Platform)	Brain Regions Analyzed	Different Subject Types
GSE 28160	HAND	GEO (GPL570)	WM	7 treated HAND subjects, 8 untreated HAND subjects, 6 controls
GSE 84422	AD	*GEO (GPL96) *GEO (GPL97) GEO (GPL570)	*FC, *BG, NA/AM	*32 subjects with AD, 19 controls; 34 subjects with AD, 19 controls

Table 2: Linear Regression Models Results Between AD vs. Control. This table lists the significant DEGs from the AD dataset shared with untreated HAND subject data. LogFC values greater than one are considered upregulated, and values less than one are considered downregulated.

Symbol	logFC	AveExpr	P.Value	adj.P.Val	B	Platforms	Regions
LINC01094	2.203553	8.2456101	7.00E-10	1.66E-06	12.09334	GPL 570	NA/AM
GALNT15	1.314648	6.4084345	7.89E-08	6.63E-05	7.48282	GPL 570	NA/AM
IL13RA1	0.962693	5.7436312	8.08E-07	0.0002847	5.225655	GPL 570	NA/AM
DDR2	1.001502	8.0978636	6.89E-08	6.07E-05	7.614065	GPL 570	NA/AM
EVI2B	1.336582	6.7128267	5.57E-07	0.00021717	5.58633	GPL 570	NA/AM
ITPR2	0.696819	6.7737886	2.53E-07	0.00013305	6.349517	GPL 570	NA/AM
MAOB	0.780507	10.141247	5.06E-07	0.00020761	5.679623	GPL 570	NA/AM
MS4A7	1.216445	7.0678849	7.93E-06	0.00114354	3.022581	GPL 570	NA/AM
DTNA	0.973504	7.9055973	5.74E-06	0.0009727	3.334435	GPL 570	NA/AM
BMP2K	0.770073	7.366542	7.38E-06	0.00111389	3.091496	GPL 570	NA/AM
CP	1.450129	5.9811838	4.55E-05	0.00355445	1.350215	GPL 570	NA/AM
CD44	1.627053	9.9312955	2.95E-05	0.0027115	1.762175	GPL 570	NA/AM
RNASE6	1.129369	6.3608359	3.05E-05	0.00275734	1.730473	GPL 570	NA/AM
AEBP1	0.930193	7.7192716	0.0001512	0.00755375	0.208958	GPL 570	NA/AM
SAMSN1	1.290342	5.9105087	4.26E-05	0.00340462	1.411982	GPL 570	NA/AM

Table 2: Continued.

ANXA1	1.217821	8.7990676	0.0001226	0.00669095	0.407316	GPL 570	NA/AM
TLR7	0.995614	4.0067311	5.25E-05	0.00387865	1.213965	GPL 570	NA/AM
FGL2	0.999921	8.0813473	0.0001201	0.00661257	0.426922	GPL 570	NA/AM
GFAP	0.372874	14.401957	3.76E-06	0.00075021	3.739906	GPL 570	NA/AM
S100A10	0.802809	10.349529	0.0002609	0.01051537	-0.30669	GPL 570	NA/AM
NUPR1	0.81781	8.9646199	0.0003861	0.01348964	-0.6757	GPL 570	NA/AM
ITPRIPL2	0.763211	4.6743973	2.34E-06	0.00053979	4.197135	GPL 570	NA/AM
ATP6V0E1	0.226589	2.9440363	0.0014468	0.03215979	-1.90975	GPL 570	NA/AM
DOCK8	0.76337	4.5680147	0.0003705	0.0131708	-0.63697	GPL 570	NA/AM
CD24	1.635793	6.6191179	0.0002111	0.00925101	-0.10663	GPL 570	NA/AM
STK32A	0.671416	4.1048961	4.19E-05	0.00336224	1.429629	GPL 570	NA/AM
DCLK1	1.238835	10.120457	7.94E-06	0.00114354	3.022147	GPL 570	NA/AM
IFIT3	-0.60901	5.476585	5.97E-06	0.00132743	3.23851	GPL 96	FC
IFIT3	-0.76255	6.3359105	1.477E-05	0.00389827	2.231482	GPL 96	FC
IFIT3	-0.68578	5.9062477	1.037E-05	0.00261285	2.734996	GPL 96	FC
ISG15	-0.68764	5.8677589	7.691E-05	0.00569488	0.815148	GPL 96	FC
STAT1	-0.3949	2.3607816	1.932E-05	0.00242516	2.121272	GPL 96	FC
FBXW7	-0.45836	8.7930551	0.0004088	0.01392838	-0.74979	GPL 96	FC

Table 2: Continued.

NRXN1	-0.50608	7.9337503	0.0027281	0.04424583	-2.49893	GPL 96	FC
FCGR1B	-0.58367	2.83776	4.057E-05	0.00380249	1.418806	GPL 96	FC
HBB	-0.74511	11.190131	0.0003314	0.01239002	-0.55416	GPL 96	FC
PART1	-0.65462	6.7144947	6.125E-06	0.00133404	3.213958	GPL 96	FC
DIRAS2	-0.76913	10.177409	2.692E-06	0.00085432	3.998798	GPL 96	FC
GBP1	-0.75003	3.2154484	2.88E-05	0.0031054	1.743075	GPL 96	FC
SNAP25	-0.56679	12.775182	1.114E-05	0.00182041	2.644057	GPL 96	FC
IFIT3	-0.76255	6.3359105	1.477E-05	0.00389827	2.231482	GPL 97	FC
DLGAP1	-0.82148	8.8806354	1.749E-06	0.0016131	4.271858	GPL 97	FC
DCLK1	-0.65612	6.5173687	6.302E-05	0.00821866	0.854234	GPL 97	FC
NRXN1	-0.59825	9.3101749	2.255E-05	0.00489439	1.828937	GPL 97	FC
GABRB3	-0.62875	8.4471402	0.0001035	0.01062345	0.385645	GPL 97	FC
GBP1	-0.77009	4.9211362	0.0001329	0.01216571	0.150332	GPL 97	FC

Table 3: Linear Regression Models Results Between Untreated HAND vs. Control. The significant DEGs from the untreated HAND dataset shared with AD subject data are listed in this table. LogFC values greater than one are considered upregulated, and values with values less than one are considered downregulated.

Symbol	logFC	AveExpr	P.Value	adj.P.Val	B
ISG15	3.491838	6.7546391	4.733E-07	0.0006011	5.940132
IFIT3	3.362526	7.0774746	2.642E-06	0.00189816	4.23041
STAT1	1.732915	9.8709457	1.339E-05	0.00585167	2.622855
C3	3.782473	8.2116405	2.964E-06	0.00207559	4.115959
C3AR1	2.52103	6.0536455	2.475E-05	0.00925724	2.017139
STAT1	1.732915	9.8709457	1.339E-05	0.00585167	2.622855
EVI2B	2.156042	5.8222471	1.4E-05	0.00606614	2.579436
HBB	-3.45334	6.1486486	4.956E-06	0.00294169	3.606494
GBP1	3.211663	5.6099893	4.139E-05	0.01298976	1.511016
SERPINB1	2.610728	7.5299795	4.289E-05	0.013235	1.475823
FCGR1B	2.704963	4.8497376	0.0003654	0.04324707	-0.61749
LINC01094	2.578449	4.7914392	0.0003015	0.03895534	-0.43099
MAOB	1.867549	8.4465423	0.0002635	0.0360399	-0.29998
CP	2.31617	6.5035535	0.0003884	0.04428432	-0.6767

Table 3: Continued.

RNASE6	1.741931	3.1948183	3.366E-05	0.01149084	1.714127
SAMSN1	2.506785	4.7847283	0.0002953	0.03876093	-0.41049
TLR7	2.999565	4.8701305	4.935E-05	0.01396574	1.337971
NUPR1	2.693328	7.5155246	4.013E-05	0.01266814	1.541333
ITPRIPL2	1.49326	8.1047011	6.129E-05	0.01564027	1.125378
SNAP25	-3.11652	10.439936	1.414E-05	0.00608004	2.569368
FCGR1B	2.704963	4.8497376	0.0003654	0.04324707	-0.61749
FBXW7	-1.90571	4.6376698	0.0002133	0.03175643	-0.09423
DLGAP1	-2.81609	8.7887179	6.598E-05	0.01645115	1.05297
DCLK1	-2.27789	5.6965361	0.0004009	0.04511252	-0.70745
NRXN1	-2.31118	8.8512038	0.0002368	0.03394861	-0.19608
SERPINB1	2.610728	7.5299795	4.289E-05	0.013235	1.475823
PLSCR1	2.306998	6.816581	4.01E-06	0.00246081	3.816263
DTNA	1.971022	8.2809792	0.0020134	0.10854948	-2.25981
GBP1	3.211663	5.6099893	4.139E-05	0.01298976	1.511016

Table 4: SAM Analysis Results from the Comparison of Untreated HAND vs. Control. The shared DEGs compared to AD vs. Control results are listed below. A positive fold change over 1 represents an upregulation, and values below 1 represent downregulated genes. Similarly, a positive score (d) equal to or greater than 1 indicates upregulation, and anything negative or below one is considered downregulated.

Gene Name	Score(d)	Fold Change	q-value(%)
LINC01094	5.4169133	6.122256923	0
GALNT15	4.8565051	3.667753316	0
IL13RA1	4.5541952	2.319959446	0
DDR2	4.4311506	4.168248095	0
EVI2B	6.3001342	4.568297935	0
ITPR2	4.2008563	2.521429483	0
MAOB	5.2620958	3.740324209	0
MS4A7	7.3702522	7.053397738	0
DTNA	5.4687061	4.018442414	0
BMP2K	5.0858631	2.82078821	0
C3AR1	5.4659184	5.883377362	0
CP	6.3139843	5.104554441	0
CD44	5.2033087	4.474071974	0

Table 4: Continued.

RNASE6	4.3409291	3.428424401	0
AEBP1	4.3755611	3.000406952	0
SAMSN1	4.0831942	5.825572282	0
ANXA1	3.9623182	4.606427525	0
TLR7	4.3453723	8.197478468	0
FGL2	4.3050999	5.829209157	0
GFAP	4.7202061	1.536085743	0
S100A10	5.5562837	6.257363736	0
NUPR1	5.4193552	6.629696382	0
ITPRIPL2	4.3020693	2.885606197	0
ATP6V0E1	4.5068678	1.609436255	0
DOCK8	4.3331141	5.385593077	0
C3	6.8946471	14.1045386	0
EIF1AY	4.7267314	3.602231856	0
UTY	4.3265237	9.380347773	0
DCLK1	-4.9159458	0.211353291	0
PART1	-4.9822129	0.283166504	0
DIRAS2	-5.0407903	0.138510617	0
GBP1	5.5305488	9.495724	0

Table 4: Continued.

SNAP25	-4.964526	0.118183242	0
IFIT3	6.0865795	10.54246699	0
FCGR1B	4.426513	6.683377472	0
HBB	-5.6245902	0.043822901	0
ISG15	6.4917531	11.53105869	0
FBXW7	-4.9446042	0.273554599	0
DLGAP1	-4.6739189	0.145543267	0
DCLK1	-4.9159458	0.211353291	0
GABRB3	-4.7797119	0.225003173	0
NRXN1	-4.9447739	0.20653191	0
SERPINB1	4.7758744	6.260780981	0
PLSCR1	6.4821609	5.611628732	0
PLSCR1	6.4767216	5.072202789	0
DTNA	5.4687061	4.018442414	0
GBP1	5.5305488	9.495724	0
FBXW7	-4.9446042	0.273554599	0
MAN1C1	4.0040713	3.845696121	0
STAT1	3.9719811	4.266228175	0

Table 5: SAM Analysis Results from the Comparison of AD vs. Control. The shared DEGs compared to untreated HAND vs. Control results are listed below. A positive fold change over 1 represents an upregulation, and values below one represent downregulated genes. Similarly, a positive score equal to or greater than one (d) indicates an upregulation, and anything negative or below one is considered downregulated.

Gene Name	Score(d)	Fold Change	q-value(%)	Platform	Region
LINC01094	6.6578092	4.495137757	0	GPL 570	NA/AM
GALNT15	4.2693039	2.2387022	0	GPL 570	NA/AM
IL13RA1	5.434101	1.901984409	0	GPL 570	NA/AM
IL13RA1	4.9027625	2.196674345	0	GPL 570	NA/AM
DDR2	4.5490281	2.050720928	0	GPL 570	NA/AM
EVI2B	4.967478	2.464669793	0	GPL 570	NA/AM
ITPR2	4.8310159	1.666934482	0	GPL 570	NA/AM
MAOB	4.8271927	1.676344812	0	GPL 570	NA/AM
MS4A7	4.5808365	2.267743033	0	GPL 570	NA/AM
DTNA	4.5528671	1.684844148	0	GPL 570	NA/AM
BMP2K	4.4042903	1.664264481	0	GPL 570	NA/AM
C3AR1	4.4006104	1.867843504	0	GPL 570	NA/AM
CP	4.3667793	2.666488994	0	GPL 570	NA/AM

Table 5: Continued.

CD44	4.28415	3.014387385	0	GPL 570	NA/AM
RNASE6	4.1927964	2.134918716	0	GPL 570	NA/AM
AEBP1	4.1556453	1.859616898	0	GPL 570	NA/AM
DDR2	4.0001111	1.938449415	0	GPL 570	NA/AM
SAMSN1	3.8170282	2.386927144	0	GPL 570	NA/AM
ANXA1	3.8053567	2.269906815	0	GPL 570	NA/AM
TLR7	3.7566192	1.94588517	0	GPL 570	NA/AM
FGL2	3.67032	1.951703033	0	GPL 570	NA/AM
GFAP	3.6586269	2.215855483	0	GPL 570	NA/AM
S100A10	3.5509986	1.702459846	0	GPL 570	NA/AM
NUPR1	3.5427208	1.720254468	0	GPL 570	NA/AM
ITPRIPL2	3.5398181	1.538617986	0	GPL 570	NA/AM
C3	3.623458	1.971693473	0	GPL 570	NA/AM
DCLK1	4.4311984	2.303211589	0	GPL 570	NA/AM
ATP6V0E1	3.4774938	1.564082952	0.036597341	GPL 570	NA/AM
DOCK8	3.4623452	1.656550042	0.036597341	GPL 570	NA/AM
EIF1AY	-6.4426054	0.125066465	0	GPL 570	NA/AM
EIF1AY	-6.1651491	0.270724866	0	GPL 570	NA/AM

Table 5: Continued.

UTY	-5.4125443	0.433605782	0	GPL 570	NA/AM
PART1	-4.2022061	0.625303164	0	GPL96	FC
DIRAS2	-3.9272622	0.577588617	0	GPL96	FC
GBP1	-3.7343483	0.574256455	0	GPL96	FC
SNAP25	-3.5946783	0.664554466	0	GPL96	FC
IFIT3	-3.5361077	0.645386208	0	GPL96	FC
IFIT3	-3.6286432	0.580570193	0	GPL97	FC
FCGR1B	-3.5185365	0.656824717	0	GPL96	FC
HBB	-3.443967	0.587286815	0	GPL96	FC
ISG15	-3.3429128	0.611151592	0	GPL96	FC
FBXW7	-4.5333508	0.6292567	0	GPL96	FC
DLGAP1	-4.3021738	0.557332016	0	GPL97	FC
DCLK1	-3.8920161	0.625016133	0	GPL97	FC
GABRB3	-3.4723019	0.636989078	0	GPL97	FC
NRXN1	-3.8323091	0.650598271	0	GPL97	FC
SERPINB1	-4.3937791	0.512203078	0	GPL96	BG
PLSCR1	-3.5008587	0.515557349	0	GPL96	BG
DTNA	-3.4046582	0.492416537	0	GPL96	BG

Table 5: Continued.

GBP1	-3.6060086	0.342399933	0	GPL96	BG
FBXW7	-3.5813755	0.531905181	0	GPL96	BG
MAN1C1	-3.5022838	0.611102027	0	GPL96	BG
STAT1	-3.3802566	0.512321518	0	GPL96	BG

Table 6: Common DEGs Between AD and HAND Subjects. The following table summarizes the results from SAM analysis and Gene Ontology Analysis. The results were obtained comparing untreated HAND vs. Control and AD vs. Control. Significant genes with a (q value < 0.05) are represented with the region and if the gene was upregulated or downregulated. The specific area analyzed is represented by abbreviations (FC: frontal cortex, BG: basal ganglia, WM: white matter). According to the DAVID bioinformatics database, the specific processes these genes are involved in are stated in this list. Based on the results, four mRNA transcripts that were significantly differentially expressed between comparisons are involved in the Type 1 interferon pathway, and they are *ISG15, GBP1, STAT1, and IFIT3*.

Gene	Function	Comparison & Up or Downregulation	Brain Region
ISG15	Defense response to virus type I interferon signaling pathway	HAND untreated vs. Control-Up AD vs. Control FC-Down	White matter Frontal Cortex Basal Ganglia
GBP1	defense response to virus interferon-gamma-mediated signaling pathway	AD vs. Control FC-Down AD vs. Control BG-Down HAND untreated vs. control-Up	Frontal cortex Basal ganglia White matter
IFIT3	defense response to virus type I interferon signaling pathway	AD vs. Control FC-Down HAND untreated vs. Control-Up	Frontal cortex White matter Basal Ganglia
PLSCR1	defense response to virus response to interferon-beta	HAND untreated vs. Control- Up AD vs. Control BG-Down	White matter Basal ganglia
STAT1	defense response to virus interferon-gamma-mediated signaling pathway type I interferon signaling pathway response to interferon-beta	HAND untreated vs. Control- Up AD vs. Control BG-Down	White matter Basal ganglia Frontal Cortex

Table 6: Continued.

DLGAP1	chemical synaptic transmission	AD vs. Control FC-Down HAND untreated vs. Control- Down	Frontal cortex White matter
FCGR1B	interferon-gamma-mediated signaling pathway	HAND untreated vs. Control- Up AD vs. Control FC- Down	White Matter Frontal Cortex
DTNA	chemical synaptic transmission Signal transduction	HAND untreated vs. Control- Up AD vs. Control BG- Down Nucleusaccumbens/amygdala-Down	White matter Basal Ganglia Nucleus Accumbens /Amygdala
NRXN1	chemical synaptic transmission Signal transduction	HAND untreated vs. Control- Down AD vs. Control FC-Down	White matter Frontal Cortex
SNAP25	chemical synaptic transmission	HAND untreated vs. Control- Down AD vs. Control FC- Down	Frontal Cortex White matter
ANXA1	Signal transduction inflammatory response	HAND untreated vs. Control- Up Nucleusaccumbens/amygdala- Up	White matter Nucleus/Amygdala
DDR2	Signal transduction regulation of bone mineralization	HAND untreated vs. Control- Up Nucleusaccumbens/amygdala- Up	White matter Nucleus/Amygdala
GABRB3	Signal transduction	HAND untreated vs. Control- Down AD vs. Control FC- Down	White matter Frontal Cortex
ITPR2	Signal transduction	HAND untreated vs. Control- Up Nucleusaccumbens/amygdala- Up	White matter Nucleus Accumbens/Amygdala
BMP2K	regulation of bone mineralization	HAND untreated vs. Control- Up Nucleusaccumbens/amygdala- Up	White matter Nucleus accumbens /Amygdala

Table 6: Continued.

C3	positive regulation of vascular endothelial growth production inflammatory response regulation of complement activation	HAND untreated vs. Control-Up Nucleusaccumbens/amygdala-Up	White matter Nucleus Accumbens/ Amygdala
C3AR1	positive regulation of vascular endothelial growth production inflammatory response regulation of complement activation	HAND untreated vs. Control-Up Nucleusaccumbens/amygdala-Up	White matter Nucleus Accumbens/ Amygdala
TLR7	inflammatory response	HAND untreated vs. Control-Up Nucleusaccumbens/amygdala-Up	White matter Nucleus Accumbens/ Amygdala

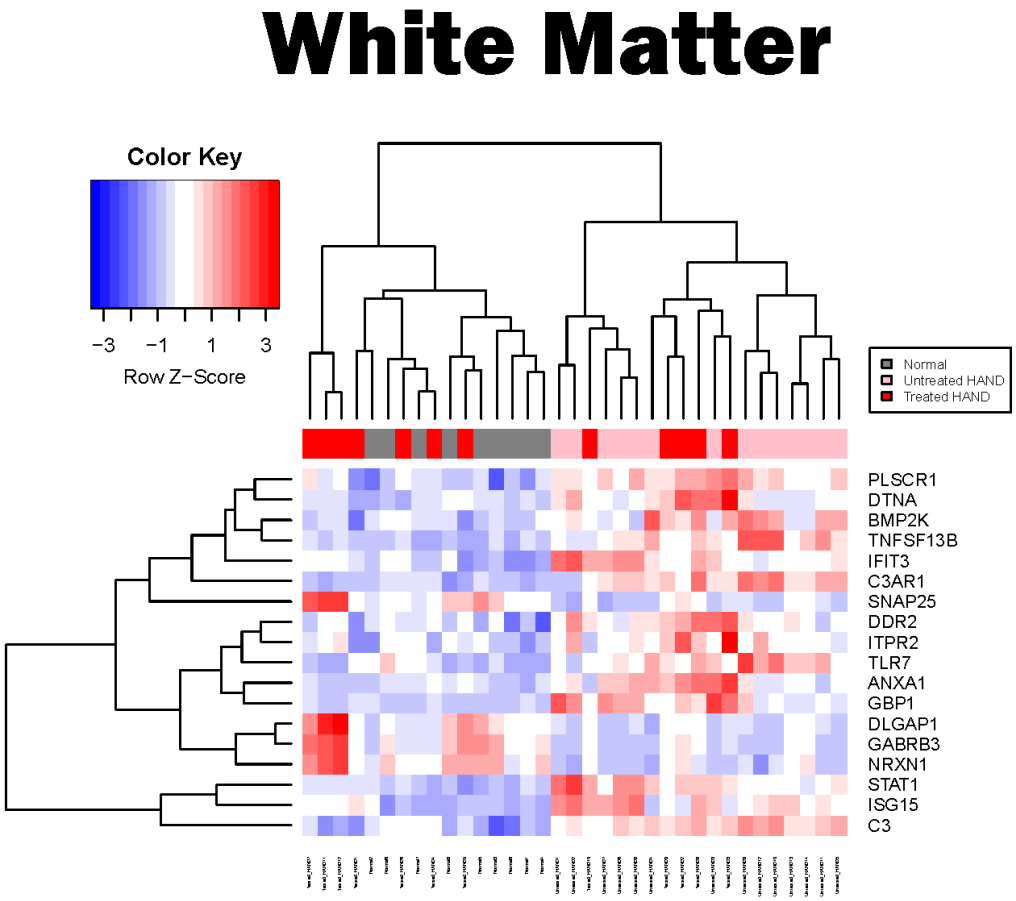

Figure 2: White Matter mRNA Expression in HAND Subjects. This heatmap represents mRNA expression after GCRMA (Bioconductor package) normalization from the white matter of HAND subjects in GSE28160. The mRNA expression represented is common markers shared between HAND and AD pathologies: *PLSCR1, DTNA, BMP2K, IFIT3, DDR2, ITRP2, TLR7, ANXA1, GBP1, SNAP25, NRXN1, DLGAP1, GABRB3, STAT1, ISG15, C3AR1, and C3*. Status of

individual subject expression is represented above the graph grey represents control groups, pink represent untreated HAND, and red represents treated HAND subjects. The figure legend includes a color key that represents the Z score. The blue color signifies downregulation, while red represents overexpression. The overexpression of mRNA transcripts can be observed in untreated HAND subjects seen in red, including *PLSCR1, DTNA, BMP2K, IFIT3, DDR2, ITRP2, TLR7, ANXA1, GBP1, STAT1, ISG15, C3AR1, and C3*. Meanwhile, the mRNA expression of *SNAP25, NRXN1, DLGAP1, GABRB3* is blue, suggesting under-expressed compared to controls.

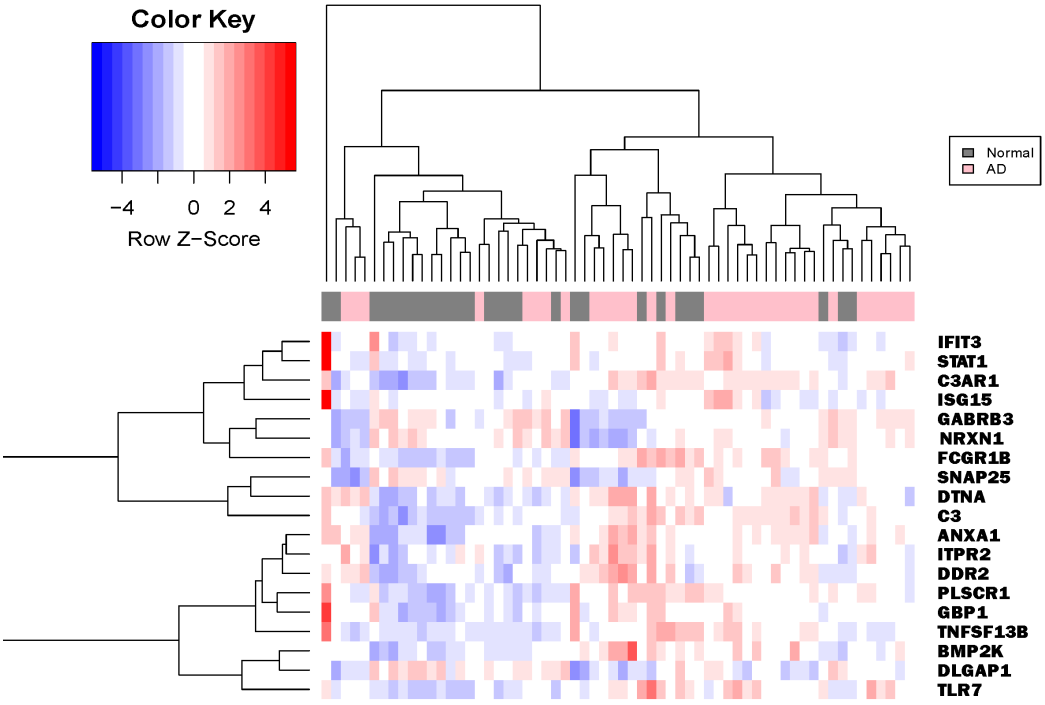

Figure 3: Nucleus Accumbens and Amygdala mRNA Expression in AD Subjects. This heatmap represents mRNA expression after GCRMA (Bioconductor package) normalization from the Nucleus accumbens and Amygdala of AD and control subjects' brains in GSE84422. The mRNA expression represented is common markers shared between HAND and AD pathologies: *PLSCR1, DTNA, BMP2K, IFIT3, DDR2, ITRP2, TLR7, ANXA1, GBP1, SNAP25, NRXN1, DLGAP1, GABRB3, STAT1, ISG15, C3AR1, and C3*. Status of individual subject expression is

represented above the graph grey represents control groups, pink represent AD subjects. The figure legend includes a color key that represents the Z score. The blue color signifies downregulation, while red represents overexpression. The figure demonstrates that mRNA expression of *DTNA* was underexpressed while transcripts *ANXA1, DDR2, ITRP2, BMP2K, C3, C3AR1, TLR7* were overexpressed seen in red.

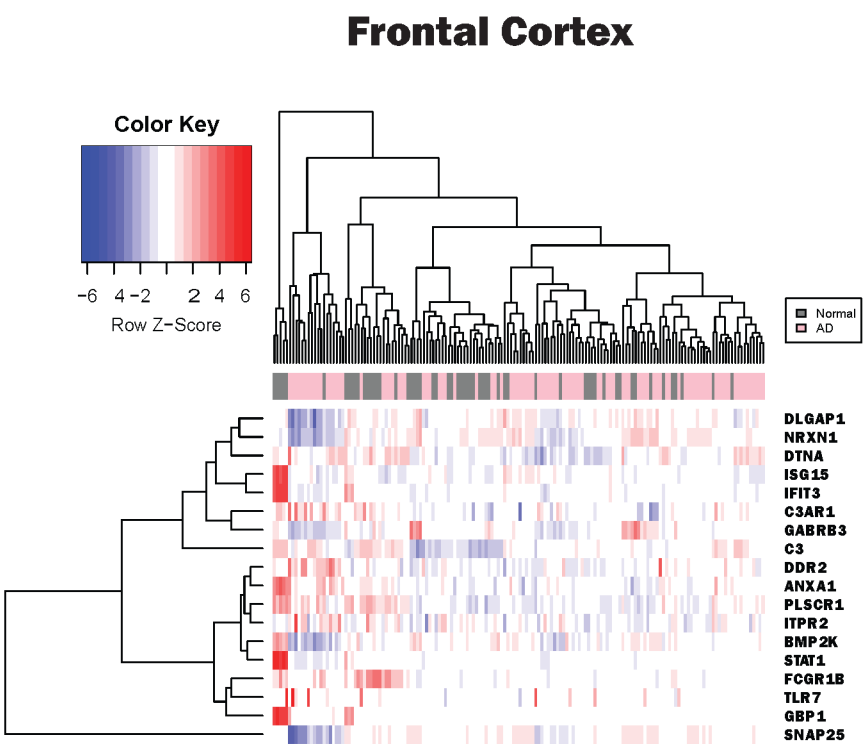

Figure 4: Frontal Cortex mRNA Expression in AD Subjects. This heatmap represents mRNA expression after GCRMA (Bioconductor package) normalization from the Frontal Cortex of AD and control subjects' brains in GSE84422. The mRNA expression described is common markers shared between HAND and AD pathologies: *PLSCR1, DTNA, BMP2K, IFIT3, DDR2, ITRP2, TLR7, ANXA1, GBP1, SNAP25, NRXN1, DLGAP1, GABRB3, STAT1, ISG15, C3AR1, and C3.* Status of individual subject expression is represented above the graph grey represents control

groups; pink represent AD subjects. The figure legend includes a color key that represents the Z score. The blue color signifies downregulation, while red represents overexpression. SAM results demonstrate the underexpression of *transcripts ISG15, GBP1, IFIT3, DLGAP1 FCGR1B, NRXN1, SNAP25, GABRB3*.

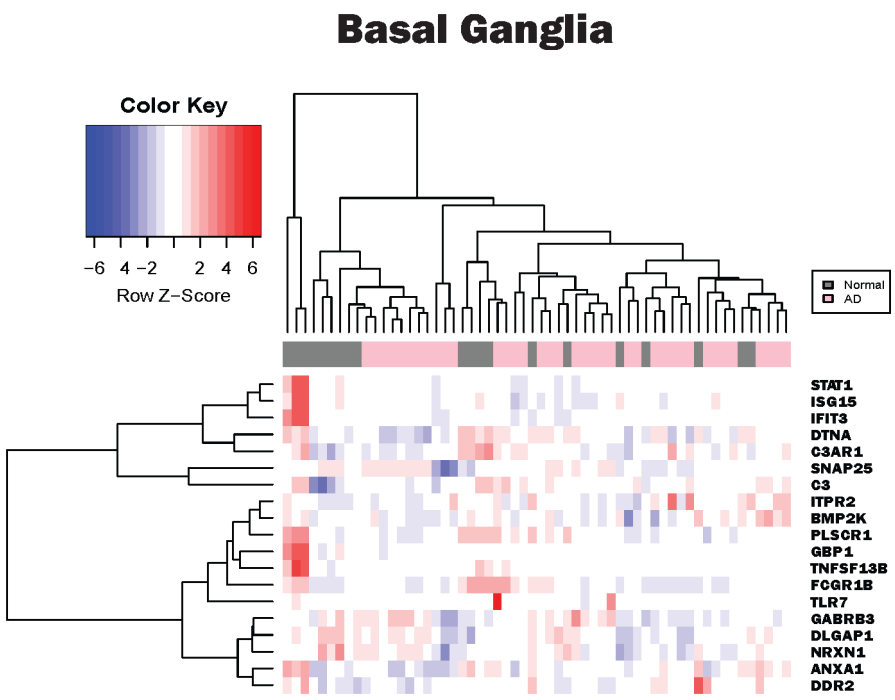

Figure 5: Basal Ganglia mRNA Expression in AD subjects. This heatmap represents mRNA expression after GCRMA (Bioconductor package) normalization from the Frontal Cortex of AD and control subjects' brains in GSE84422. The mRNA expression represented is common markers shared between HAND and AD pathologies: *PLSCR1, DTNA, BMP2K, IFIT3, DDR2, ITRP2, TLR7, ANXA1, GBP1, SNAP25, NRXN1, DLGAP1, GABRB3, STAT1, ISG15, C3AR1, and C3*. Status of individual subject expression is represented above the graph grey represents control groups, pink represent AD subjects. The figure legend includes a color key that

represents the Z score. The blue color signifies downregulation, while red represents overexpression. Based on SAM results *ISG15, GBP1, STAT1, PLSCR1, DTNA* were under-expressed in the Basal Ganglia of AD subject brains.

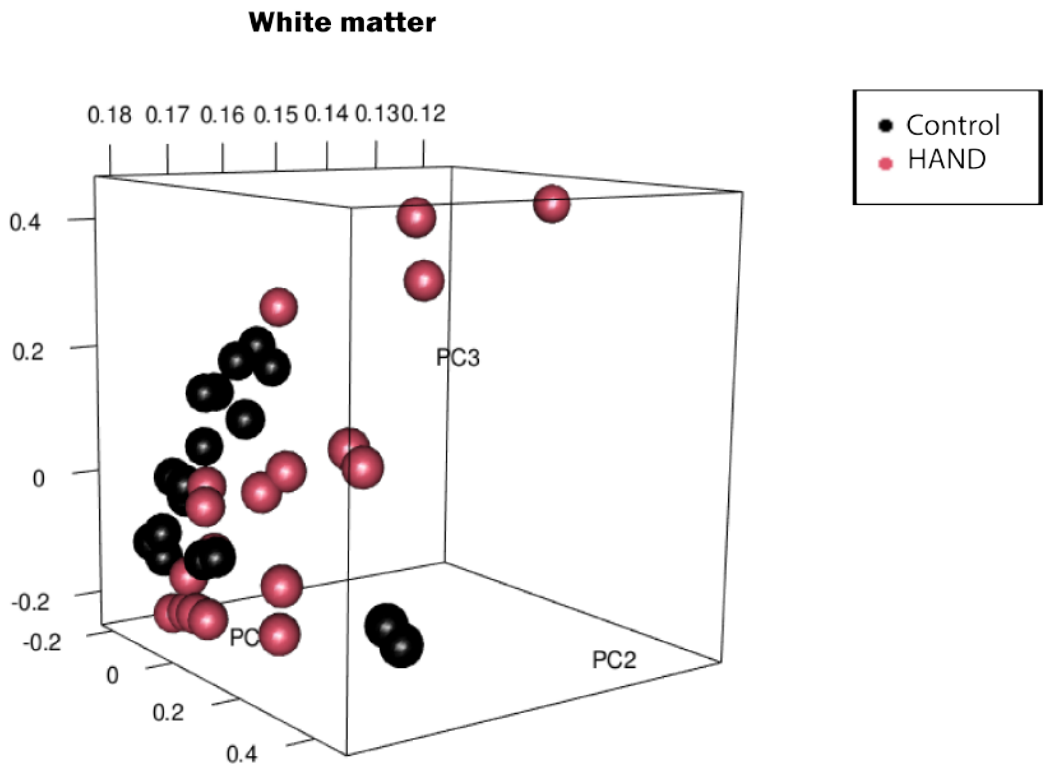

Figure 6: Individual HAND Subject Expression in the Dataset. Principal Component Analysis of the controls and groups within the white matter of untreated HAND patients from GSE28160. Details of the platforms and patients' data can be found in table 1. Clusters of spheres represent similar expressions in subjects the further they are apart, the more their expression differs.

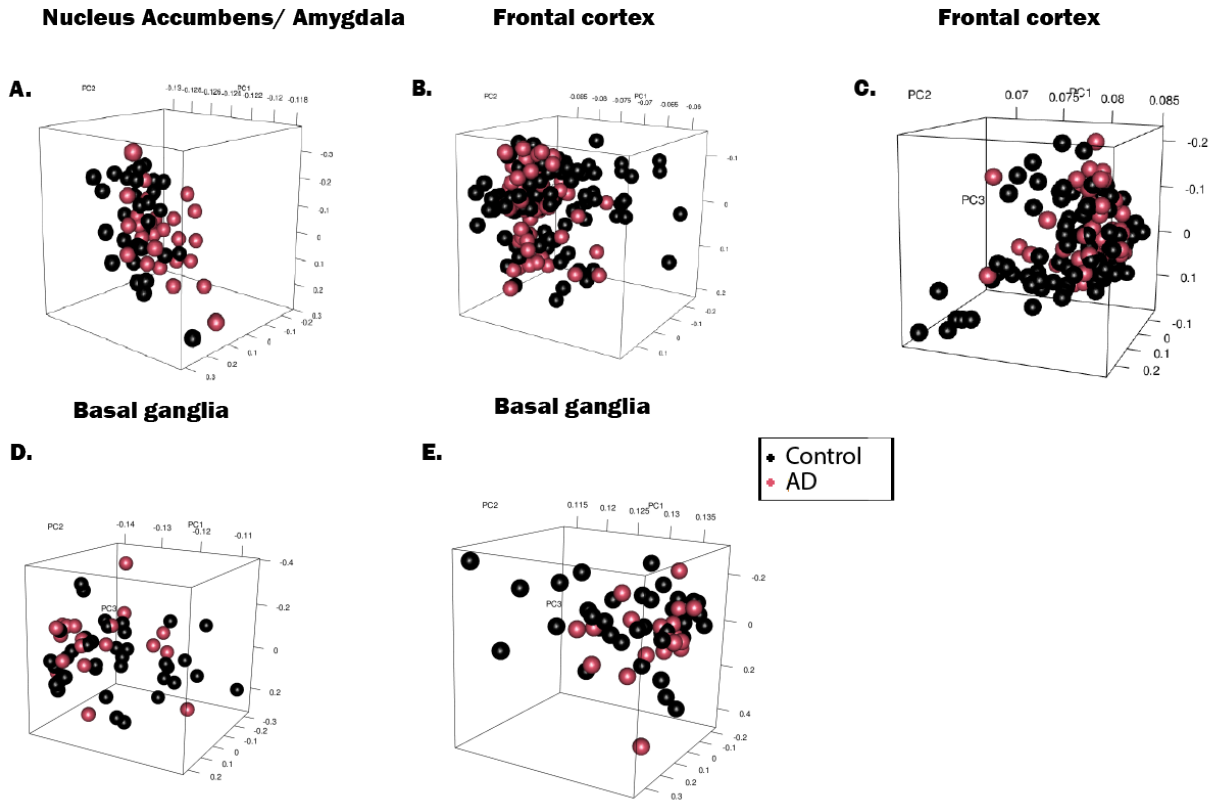

Figure 7: Individual AD Subject Expression in the Dataset. Principal Component Analysis of the controls and the three platforms that make up dataset GSE84422. Details of the platforms and patient data can be found in Table 1. Figure 7A represents the data derived from the nucleus accumbens and amygdala. This shows clustering in the negative direction of the PC1 axis where both control and AD subject group seem to cluster together in the same area on the axis. AD subject data, however, spreads out more, and some subject data can be seen on the positive end

of the PC1 axis, meaning there is more variability of the subject data. Figure 7 B-C represents the frontal cortex data. Both plots represent clusters of data on opposite ends of the PC1 axis. Still, both contain subject data clustered together and show some variability among control groups on the PC2 axis. Figure 7D-E represents the basal ganglia subject data which displays more variability in Figure 7D with no clear clusters. However, Figure 7E depicts clusters on the positive end of the PC1 plot and towards the negative end of the PC2 axis.

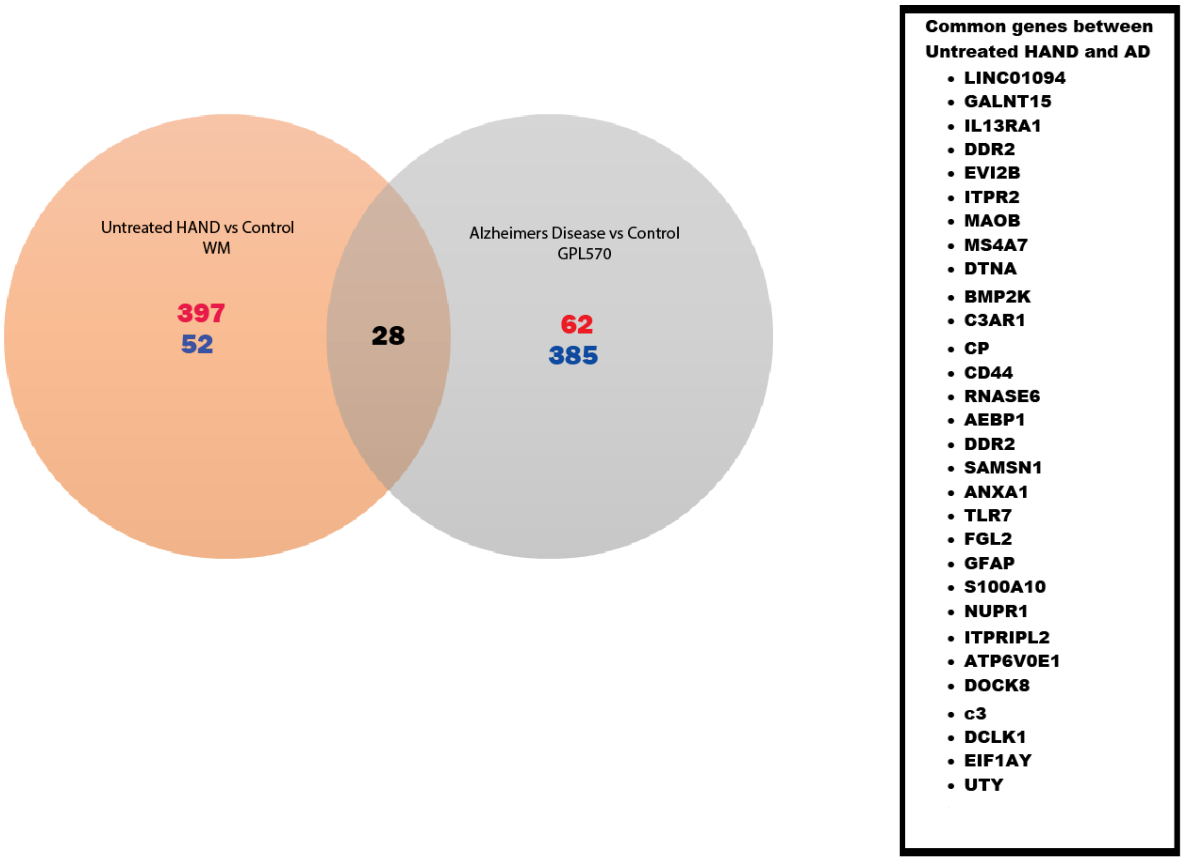

Figure 8: Dysregulated Genes in Untreated HAND and AD Subjects. This Venn diagram represents the SAM results considered significant (q-value= <.05). The results were generated using "Two unpaired analysis" independently comparing untreated HAND vs. Control and AD vs. Control. The white matter of untreated HAND subjects had 397 upregulated genes and 52 downregulated genes. AD subjects' nucleus accumbens and amygdala resulted in 62 upregulated and 385 downregulated genes. The 28 genes that were dysregulated in both diseases are mentioned to the right of the Venn diagram.

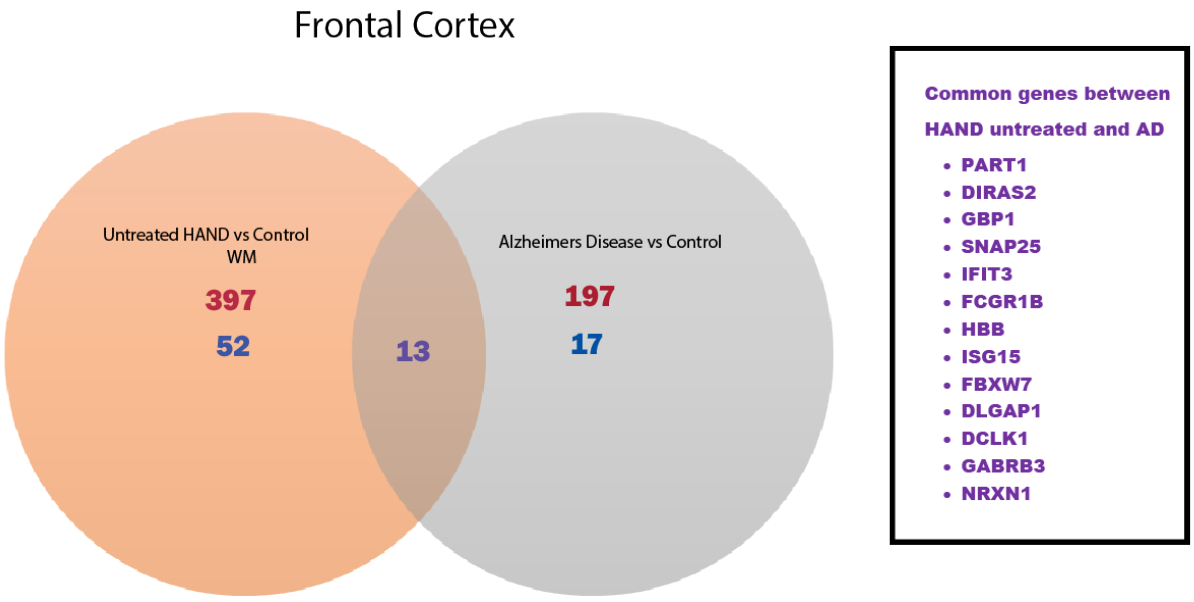

Figure 9: Dysregulated Genes in Untreated HAND and AD Subjects. This Venn diagram represents the SAM results considered significant (q-value= <.05). The results were generated using "Two unpaired analysis" independently comparing untreated HAND vs. Control and AD vs. Control**.** The Frontal cortex regions of AD subjects had 197 downregulated genes and 17 upregulated genes. The white matter of untreated HAND subjects had 397 upregulated genes and 52 downregulated genes. The 13 common genes that were dysregulated in both diseases are listed in purple on the right of the Venn diagram.

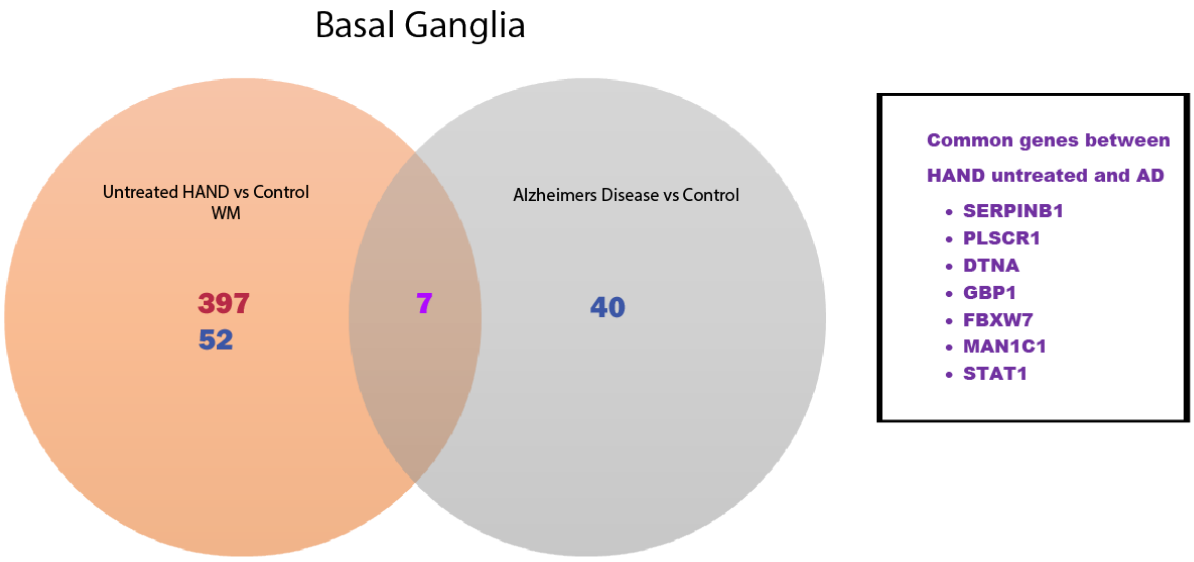

Figure 10: Dysregulated Genes in Untreated HAND and AD Subjects. This Venn diagram represents the SAM results considered significant (q-value= <.05). The results were generated using "Two unpaired analysis" independently comparing untreated HAND vs. Control and AD vs. Control**.** The Basal Ganglia regions of AD subjects had 40 downregulated genes based on mRNA expression. The white matter region of untreated HAND subjects had 397 upregulated genes and 52 downregulated genes. The seven genes shared between untreated HAND and AD are listed in purple to the right of the Venn diagram.

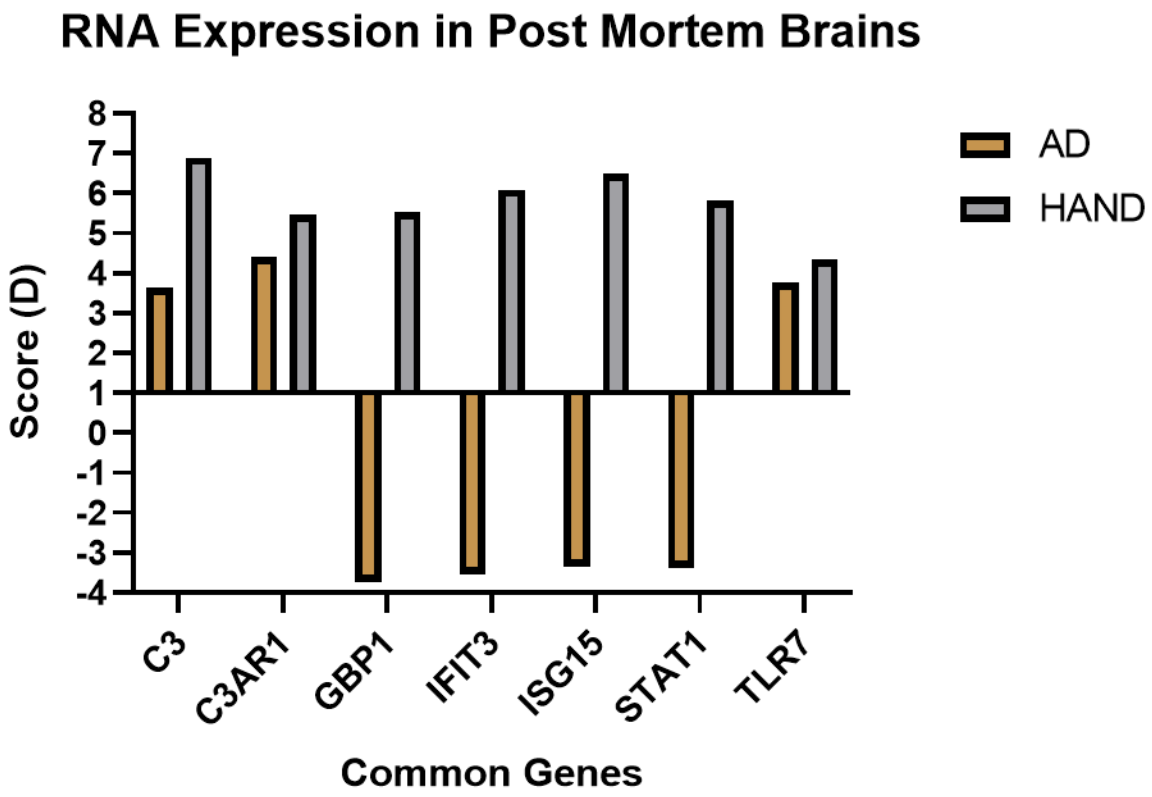

Figure 11: Dysregulated RNA in AD in HAND**.** SAM results are represented in this figure in which we could observe a difference in expression of type 1 interferon genes. The results were derived from the SAM Analysis using "two unpaired analyses" independently using "Control vs. AD" and "Control vs. HAND." The Score (D) with a baseline of 1, meaning anything above 1, is considered upregulated. Therefore, anything below 1 represents a downregulation. The gray represents AD data, and the orange represents untreated HAND data.

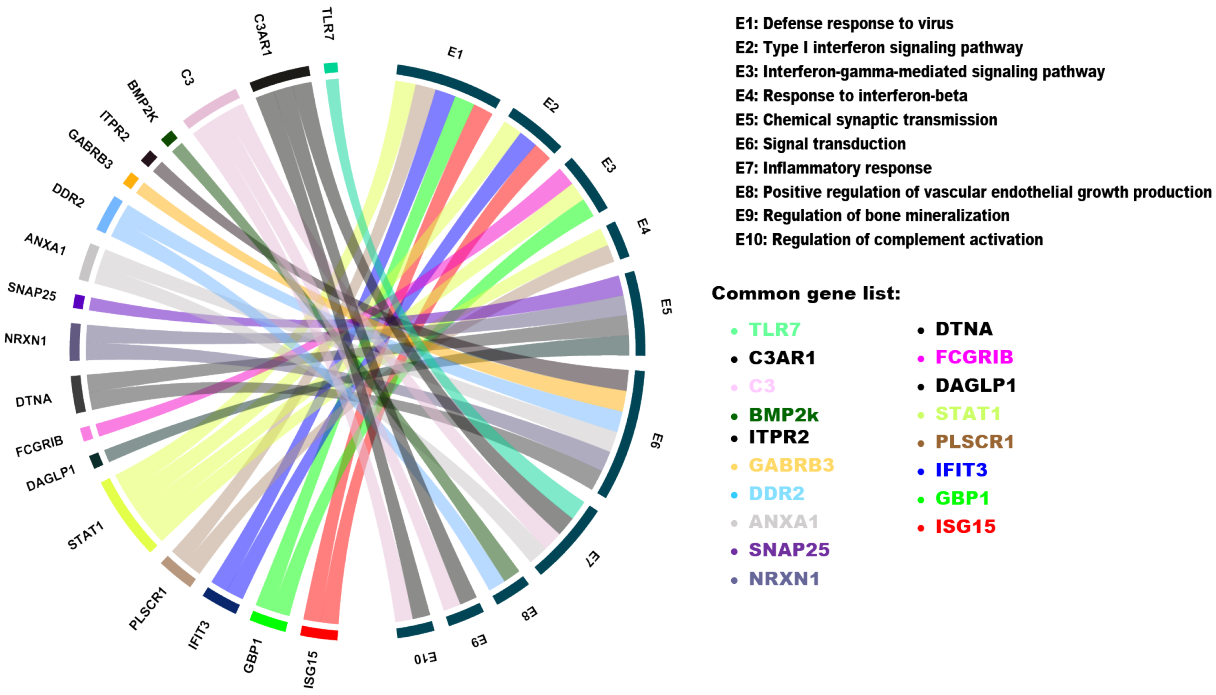

Figure 12: Common Gene Function using DAVID. This chord diagram represents the common genes generated from the SAM Analysis results and submitted through DAVID for the Gene ontology analysis. This allowed for identifying the specific processes affected in both AD and HAND. Each gene is connected to its respective function through a chord.

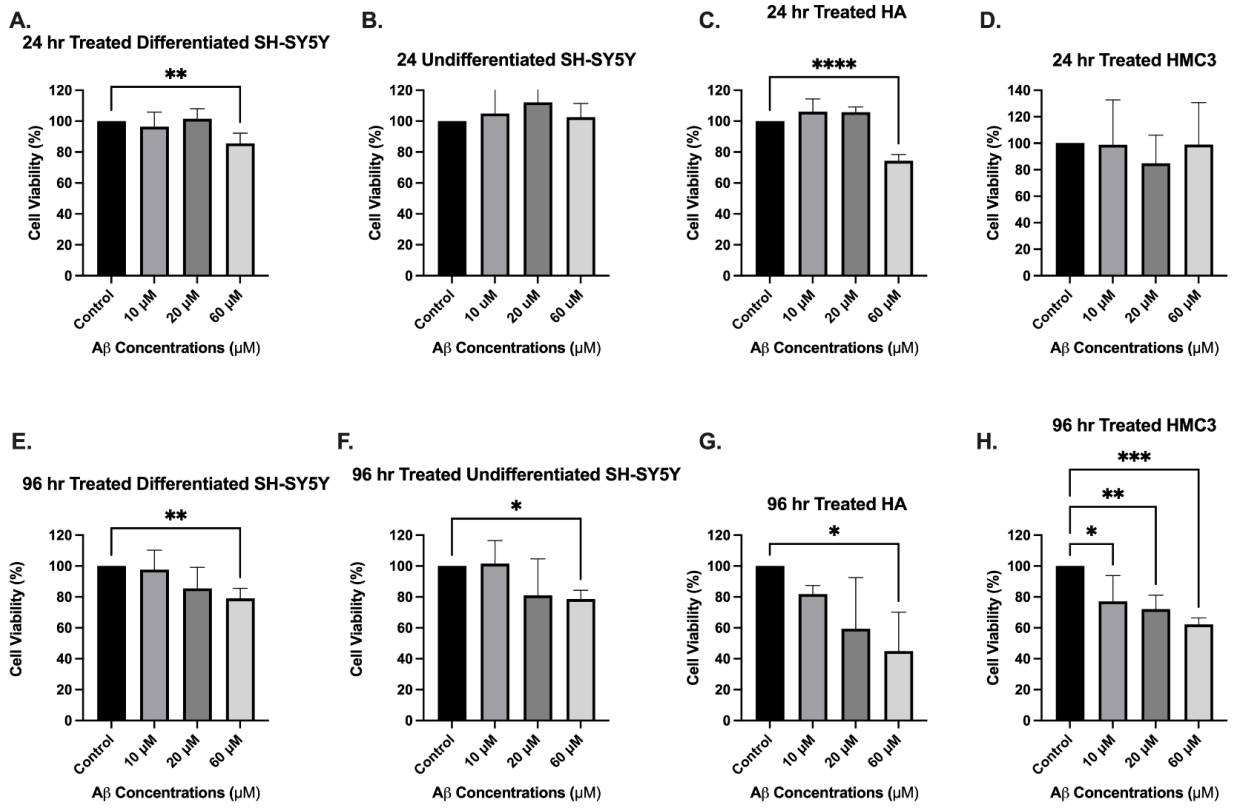

Figure 13: AD Model Cell Viability. MTS results show that there is a significant reduction in cell viability at 60µM at 96 hours for differentiated (p=0.0065, 95% C.I.=[5.734,36.26]) and undifferentiated SH-SY5Y (p=0.0435, 95% C.I.=[0.5453,42.16]) , HA (p=0.0158, 95% C.I.=[10.56,99.53]) , and HMC3 (p=0.0004, 95% C.I.=[19.38,56.09]) cells treated. Here Dunnets multiple comparison significance is annotated with (*) in which $p \leq 0.05$ (*), $p \leq 0.01$ (**), $p \leq$ (***). For more details on statistical analysis refer to results section.

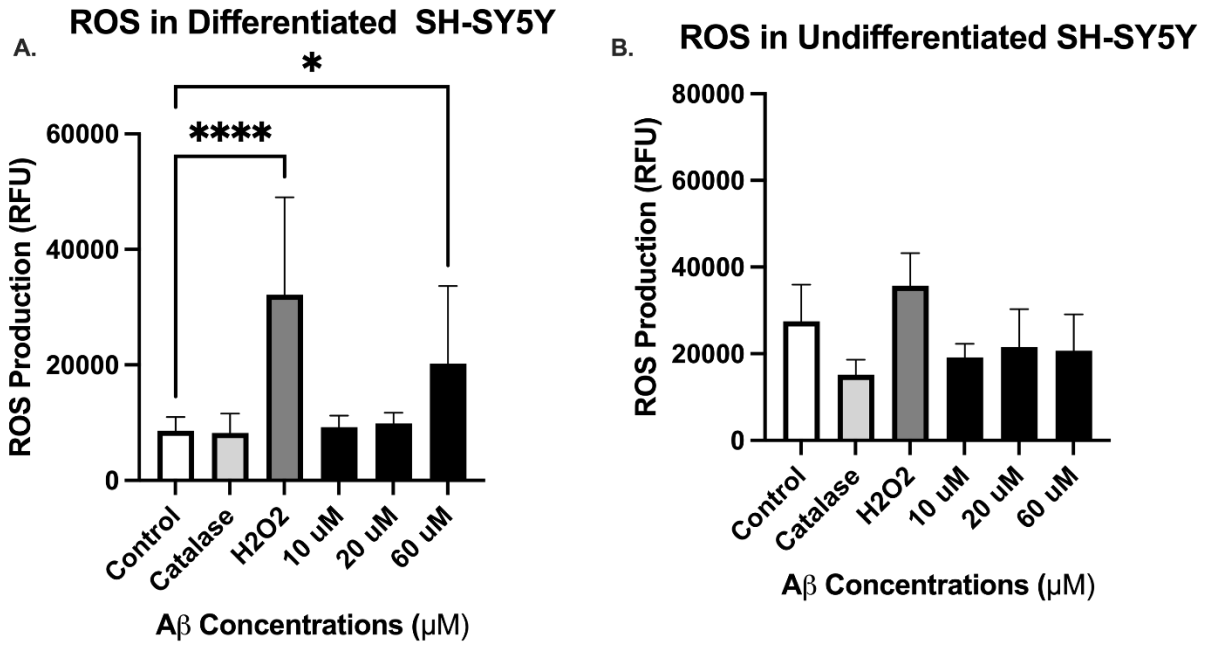

Figure 14: Reactive Oxygen Species in Aβ Treated Cells. Differentiated and undifferentiated cells were treated with Aβ, catalase was used as a negative control, and H_20_2 was used as the positive control. After 18-hour incubation with Aβ, there was no significant increase in ROS production in undifferentiated cells. Differentiated cells showed a significant difference between Control vs. H_20_2 ($p=<0.0001$, 95% C.I.=[-35272,11779]) and Control vs. 60μM ($p=0.0124$, 95% C.I.=[-21172,1990]). Dunnett's multiple comparison significance is annotated with (*) in which $p \leq 0.05$ (*), $p \leq 0.01$ (**), $p \leq$ (***).

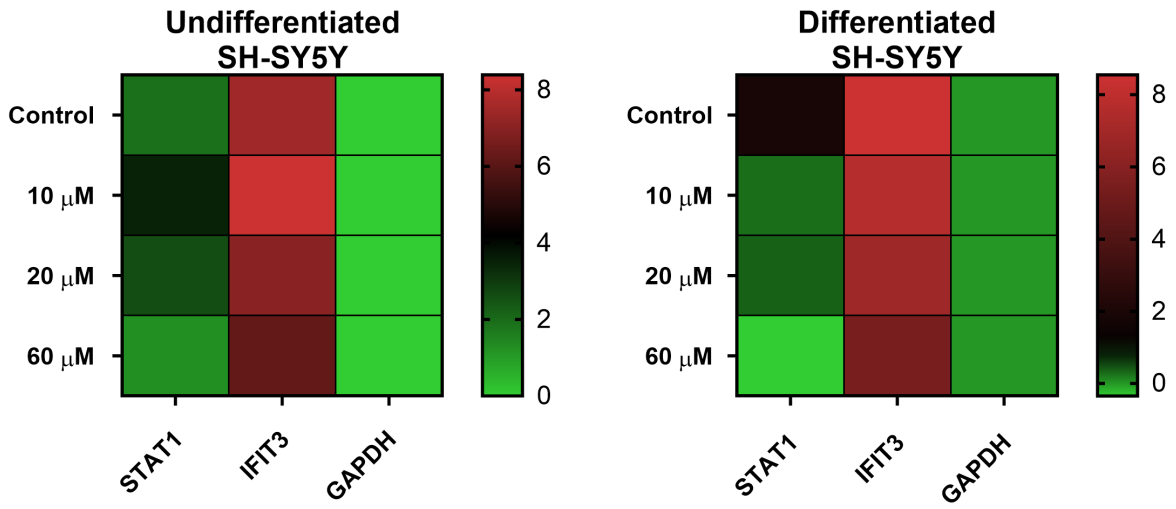

Figure 15: RNA Expression in SH-SY5Y Cells. No significant results were found through RT-PCR in undifferentiated (p=0.9709) and differentiated SH-SY5Y cells (p=0.9566) treated with Aβ for 96 hours. Here the delta CT values are used to represent the RT-PCR data. The greater the mean difference is to the housekeeping gene *GAPDH.* There is no significant difference between *STAT1* and *IFIT3* in undifferentiated and differentiated cells.

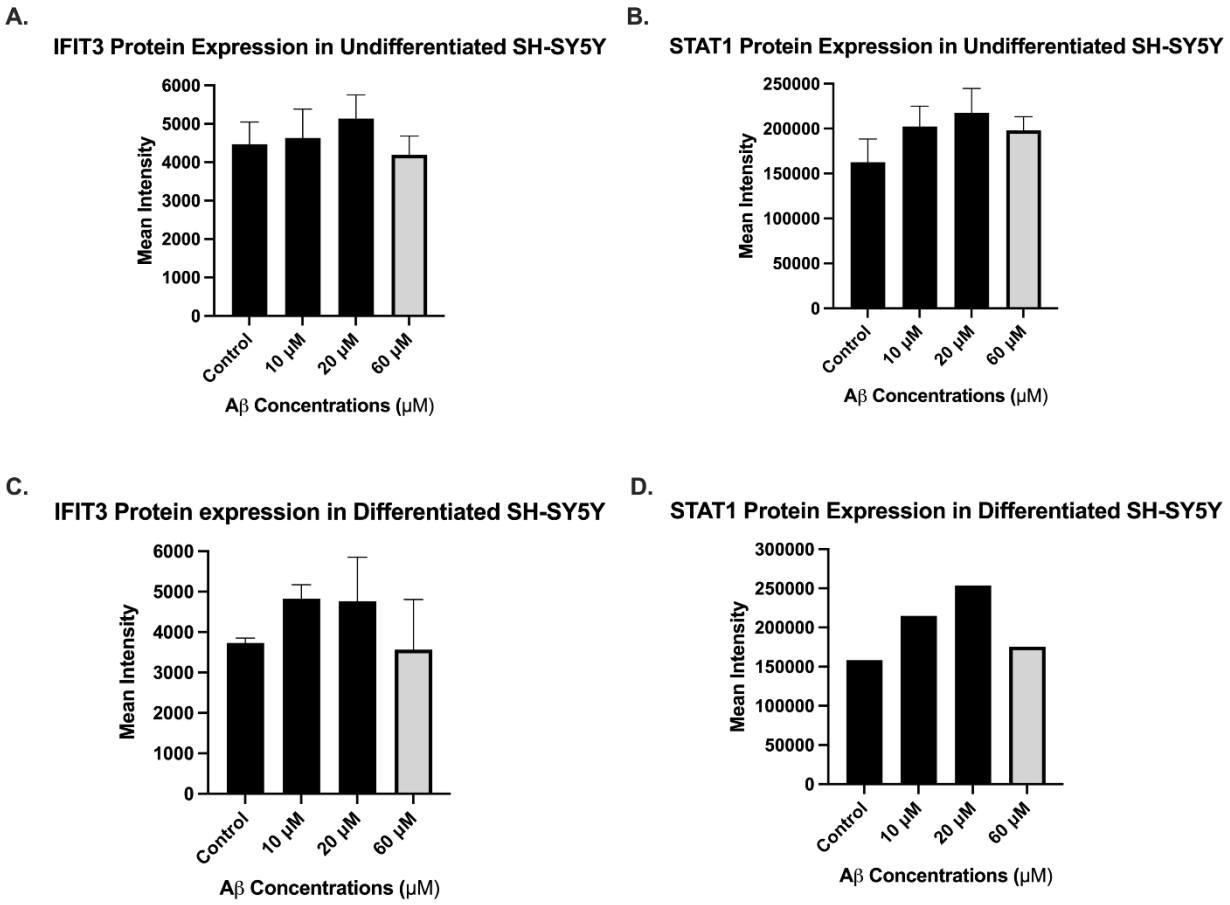

Figure 16: Protein Expression in Aβ Treated SH-SY5Y. Flow cytometry results show no significant difference in protein expression for IFIT3(p=0.3578) and STAT1(p=0.2526) in undifferentiated SH-SY5Y. Similarly, IFIT3 (p=0.4029) and STAT1 did not show any significant results undifferentiated SH-SY5Y. However, there is a reduction of IFIT3 below control levels in cells treated with 60µM of AB. Despite the increase in the number of transcripts

produced, this data suggests an impairment in translation machinery. STAT1 protein levels are lower 60μM compared to lower concentrations suggesting a slower translation rate.

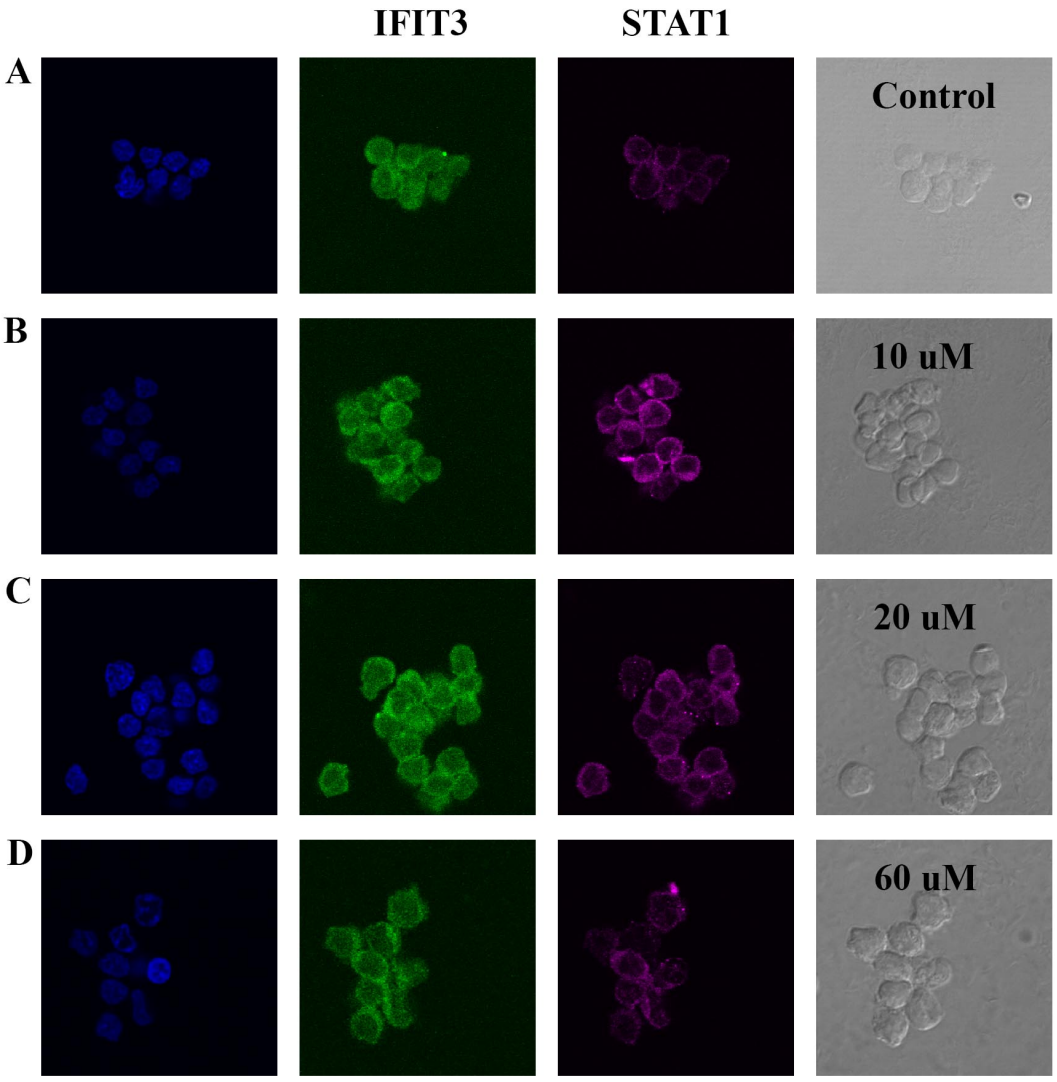

Figure 17: Protein Expression in Undifferentiated SH-SY5Y. Neuroblastoma (SH-SY5Y) cells that were grown in control (A), 10µM (B), 20µM (C), and 60µM (D) Aß for 96 hours. Cells were trypsinized, washed, fixed, and labeled with anti-IFIT3 (green, FITC) and anti-STAT1 (red, Alexa647). A portion of cells were selected for imaging using a confocal microscope under

identical exposure (A-D). The other cell portions were used in flow cytometry experiments. Panels A-D illustrates that by increasing the concentration of Aß from 10 to 60µM, the IFIT3 and STAT1 expressions initially increase and then decrease at the concentration of 60µM.

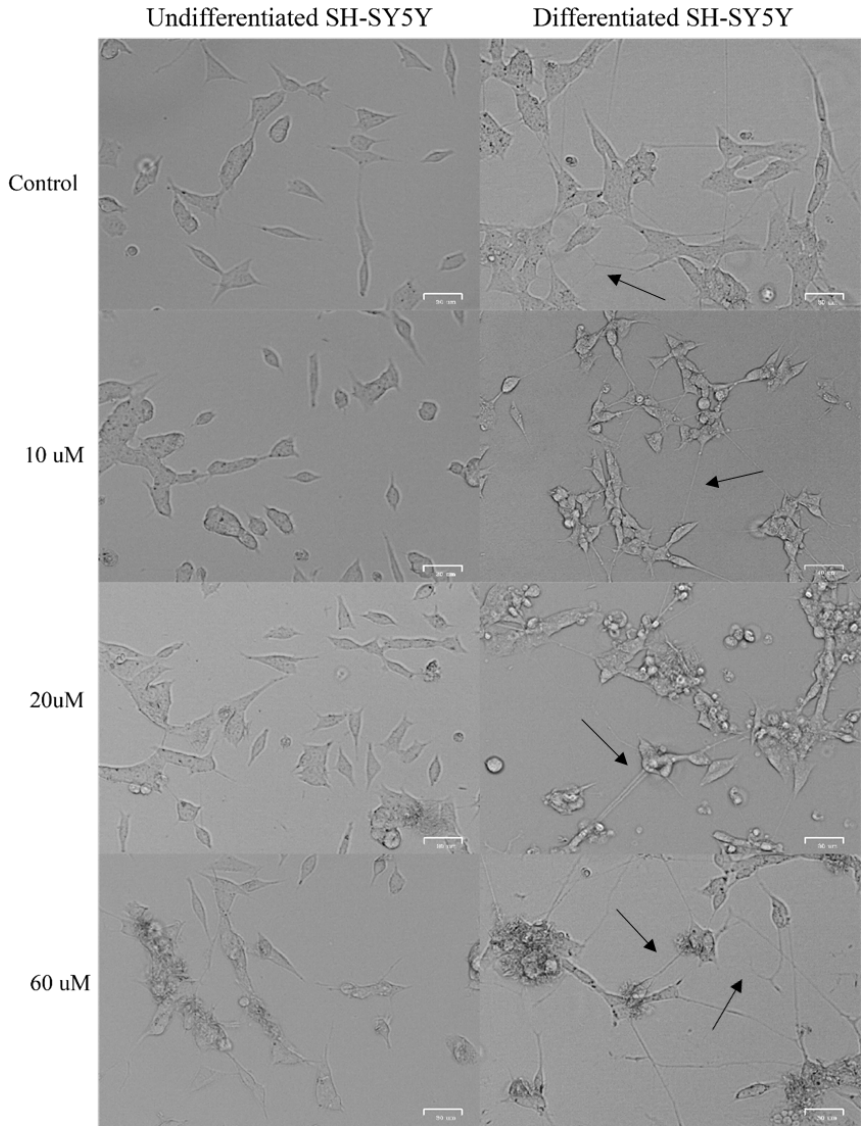

Figure 18: 96-hour Aβ Treatment in SH-SY5Y Cells. After 96 hours, cells treated with 60μM of Aβ showed a significant reduction in cell viability and a significant production of ROS compared to other concentrations.

CHAPTER III

SUMMARY AND CONCLUSION

Identification of Common Biomarkers in AD and HAND

The neurodegeneration observed in populations suffering from HAND and AD share common characteristics, including neuroinflammation and Aβ deposition in the CNS (Pulliam et al., 2019; Stern et al., 2018). Considering these neuropathologies are relatively common among the aging population with HIV-1 infection, it has become increasingly difficult to detect and distinguish between these two diseases based on their symptoms (Kahn et al.,2019; Milanini et al., 2019; Pulliam et al., 2019). To biologically characterize these two diseases and find a potential biological indicator (Kodidela et al., 2019), it is important to understand the underlying molecular pathways involved in these two diseases, especially in co-existing conditions (Rubin et al., 2019). Therefore, the present study has taken advantage of the existing RNA expression datasets from post mortem brains samples to investigate a set of common and distinctive gene biomarkers for HAND and/or AD. The AD, untreated HAND, and treated HAND data were initially compared to healthy controls considering that AD and HAND will have similar gene expression compared to control. Using independent results with this same analysis, we were able to perform this type of comparison. Due to the lack of datasets containing cART treated HAND patient transcriptome data, the treatment was not a factor we considered in our analysis. Our

objective was to identify common mRNA transcripts differentially expressed between HAND and AD subjects. The basal ganglia and the frontal cortex regions of the AD patients' post-mortem brains were investigated in this study. The current study helped to identify signaling pathways that are dysregulated and may be crucial in the development of the neuropathology seen in AD and HAND.

Type 1 interferons are part of the innate immune response that interferes with a viral infection. Toll-like receptors allow cells to recognize bacteria, viruses, and cellular debris and activate interferons' transcription. The current study has shown an upregulation of *TLR7* in untreated HAND and AD postmortem samples. TLR7 is involved in recognition of viruses, double-stranded RNA, and single-stranded RNA, and its activation results in downstream transcription of type 1 interferons, including type 1 interferons α/ß (IFN α/ß) (Meier et al.,2007). IFN α/ß and its receptor, an IFNAR complex, recruits STAT1 and STAT2 for phosphorylation, creating a heterodimer that forms a complex with IRF9 known as ISGF3 (Borden et al., 2007; Platanias, 2005). This complex is then translocated into the nucleus, activating the transcription of interferon-stimulated genes (ISGs) as part of the immune response (Zhao et al., 2013). This interferon response is known as the JAK-STAT pathway signaling cascade to promote neuroinflammation. Therefore, it is important to investigate how to regulate the immune response to avoid dysregulated forms of inflammation in the brain commonly observed in neurodegenerative diseases (Taylor et al., 2014).

The results from the DAVID analysis allowed the identification of two common interferon pathways that were found dysregulated in both AD and HAND (Figure 12). Three genes were identified involved in the type I interferon pathway, including *STAT1*, *IFIT3*, and

ISG15. Several genomic and transcriptome analysis studies have indicated that genes like *ISG15*, STAT1, and IFIT3 can, directly and indirectly, regulate HAND or AD (Dansokho et al., 2016; Gomez et al., 2020; Hsu et al., 2013; Hsu et al., 2014; Kuffor et al., 2019; Nazarian et al., 2019; Zhang et al., 2015). However, their underlying mechanisms and contribution to neuropathology are not well understood. Our study has established that in untreated HAND subjects, the expression of *STAT1*, *IFIT3*, and *ISG15* was upregulated as expected due to viral infection. However, in AD postmortem brain samples, there was downregulation of *STAT1*, *ISG15*, and *IFIT3*. This is supported by another study analyzing the post-mortem AD brain, where decreased *IFN-α* and *IRF7* levels suggest an impaired immune response. They also demonstrated that the expression of genes varies in distinct regions of the brain, which may have different consequences due to region- and gene-specific functions (Romagnoli et al., 2020). In our analysis, the frontal cortex and basal ganglia regions were analyzed based on their involvement in motor commands and executive function, respectively.

The type 1 interferon response can have harmful or beneficial effects that have been seen in various neurodegenerative diseases. It has been observed to induce anti-inflammatory effects in multiple sclerosis and is associated with chronic inflammation in AD. However, our results show a downregulation of *STAT1* in AD postmortem brains. It has been observed that *STAT1* deficiency leads to the activation of secondary pathways that are associated with severe neurological effects (Wang et al., 2002). Previous studies have aimed to understand the function of type I interferon in the CNS and confirm the upregulation of interferons in the presence of Aβ due to chronic stimulation (Roy et al., 2020; Taylor et al., 2014). However, our results showed a downregulation of STAT1 in AD postmortem brains. Another study supported this observation

where initial upregulation of interferon response in microglia was downregulated within six days of infection with the neurotropic virus, indicating impaired IFN-γ response (Hwang & Bergmann, 2020). The present study has identified four genes *CD44*, *FCGR1B*, *GBP1*, and *STAT1*, from the common genes of AD and HAND that are involved in the IFN-γ mediated signaling pathway. Previous studies have investigated patients' nitric oxide (NO) levels in different stages of AD in both microglia and astrocytes, which have neurotoxic effects in the brain and contribute to AD pathology (Belkhelfa et al., 2014). The study also identified that IFN-γ and tumor necrosis factors (TNF) were needed to induce NO production. However, the mechanism of how these cytokines regulate the production of NO and how this can potentially reduce the inflammation observed in AD pathology needs further investigation (Belkhelfa et al., 2014). Another study has suggested that experimental autoimmune encephalomyelitis (EAE) induced IFN-γ signaling can have a protective effect through STAT1 in immune cells of the CNS. In the absence of *STAT1*, cells suffered from a severe form of EAE. STAT1 deficiency observed in our analysis may lead to detrimental effects seen in EAE CNS in vitro models (Lee & Chanamara, 2012). However, IFN-γ produced by CD8+ T cells and microglia has been observed in the brains of mice and patients with AD (Unger et al., 2020). The type II interferon pathway requires a STAT1 homodimer that translocates into the nucleus, where it can bind to cis-regulatory elements known as gamma activating sequences (GAS) elements that can either activate or suppress interferon-regulated genes (Roshan et al., 2017). A study observed that phosphorylated STAT1 allows tau fragment (1-368) to bind and activate the transcription of *BACE1*. It was observed that this mechanism is dependent on the presence of the

amyloidprecursor protein (586-695), which regulates the phosphorylation of kinases SGK1 and JAK2, which are both activators of STAT1 (Zhang et al., 2018).

Some of the downstream ISGs that deserve further investigation regarding their roles in the CNS include *IFIT3* or *ISG60* that are expressed downstream of the JAK-STAT pathway. It has been observed that IFN-β secretion activates the production of *IFIT3*, which can then regulate the downstream production of chemokine *CXCL10* (Imaizumi et al., 2016). IFIT3 can function as an inhibitor of cellular and viral processes, cell migration, proliferation, signaling, and viral replication; however, a better understanding of AD pathology is needed (Pidugu et al., 2019). On the other hand, *ISG15* has been identified as an interferon-stimulated gene since its expression is induced in response to type I interferons or lipopolysaccharide treatment (Malakhova et al., 2002; Zhang et al., 2015). ISG15 activity is tightly regulated by specific signaling pathways that play an innate immunity role. A study demonstrated that ISG15 could negatively regulate the type 1 interferon response through USP18 stabilization (Zhang et al., 2015). This study showed an increase in *ISG15* untreated HAND brain samples. This finding is supported by a previous study that analyzed cerebrospinal fluid (CSF) and post mortem brain samples of people who had HAND, identifying increased levels of *ISG15* in the early stages of HAND (Fields et al., 2013). This suggests that the regulation of downstream activation of ISGs in response to type 1 interferons may benefit people with HIV-1. Since both of these ISGs are activated downstream of STAT1 in the Type 1 interferon response, understanding how these genes may regulate inflammation or other factors contributing to the neurodegeneration seen in the CNS may be helpful for the development of therapeutic drugs.

A recent study has indicated that the interferon response can directly or indirectly regulate other mechanisms involved in neurodegeneration regarding *C3* and *C3AR1*. These two genes are involved in the complement cascade pathway and were both found upregulated in AD and HAND subjects. This study demonstrated that interferons can regulate microglia-mediated synapse loss through complement cascade components (Roy et al., 2020). However, further investigation is needed to fully understand the contribution to neurodegeneration (Roy et al., 2020). Innate immunity can be regulated through the complement pathway in which the cleavage of C3 into C3a and C3b is followed by binding to C3AR1 and CR3, respectively. It is expressed in the central nervous system and is associated with aging and neuropathology (Litvinchuk et al., 2018). The C3-C3aR has been observed to mediate mechanisms involved in immune response and neuron interactions involved in network function and Aβ pathology. However, the interactional relationships between neurons, astrocytes, and microglia need to be further understood. This study showed that C3aR has a critical role in mediating CNS immune hemostasis and tau pathology through the JAK-STAT pathway (Litvinchuk et al., 2018). In addition, levels of IL-6 have been observed in the brains of AD patients. The presence of Aβ can activate the *NALP3* inflammasome that will cause the secretion of IL-1ß and IL-6, respectively, and also induce the transcription of acute-phase response proteins like C3 (Ayton, 2020). The *C3* gene expression has been observed in the brains of HAND, where *NF-kB* induction of *IL-6* activates the *C3* gene. This contributes to inflammation and cognitive dysfunction in people with HIV-1 infection (Nitkiewicz et al., 2017). Further research is needed to investigate and compare the mechanisms involved in regulating C3 and C3AR1 in the CNS of AD and HAND subjects.

Despite the sample size, our data supports multiple studies that recognize type 1 and type II interferon signaling pathways related to HAND and AD. In summary, it is important to understand further the mechanism of these pathways and how they mediate neuronal plasticity through astrocyte and microglia activation. *STAT1* is a gene involved in interferon response; however, more research is needed to understand its regulation in AD pathology. Some of the genes downstream of *STAT1* are *ISG15* and *IFIT3*, which are involved in innate immunity. The expression levels of these mRNA transcripts were dysregulated in different brain regions. This may be worth further investigation to understand better the mechanisms in which they may elicit inflammation in the central nervous system. Due to the limited available data, treatment was not considered important in HAND data analysis. However, since most people with HIV receive the treatment, it would be ideal for collecting data from larger cohorts receiving treatment in the future.

Overall, the transcriptome profiles of the brains of people with HAND and AD highlight opposite expressions of RNA involved in type 1 interferon signaling, including *STAT1*, *ISG15*, and *IFIT3*. The expression of genes involved in this immune response varies in different neurodegenerative diseases. It is suggested to be involved in the different neuropathologies that lead to cognitive decline. A limitation of this study is that we did not consider age as a factor for comparison due to the small sample size. It has been observed that there are age-related differences in brain atrophy in AD brains (Senguko, 2020). Also, epigenetic histone modifications that are associated with age have been implicated in AD (Nativio et al., 2018). It would be interesting to see the different levels of gene expression at different stages of the disease. Further research is needed to confirm these observations using *in vitro* or *in vivo* models

to understand further the mechanisms involved in the progression of neurodegenerative diseases. Nonetheless, to the best of our knowledge, this is the first comprehensive report comparing the epigenetic mechanism of AD and HAND from two established RNA datasets.

Type 1 Interferon Gene Expression in *in vitro* AD Model

To further understand the regulation of *STAT1* and *IFIT3* in an AD, an *in vitro* model was established based on published data (Lattanzio et al., 2016; Li et al., 2019; Yu et al., 2014). Previously described in this article, Aβ is one of the hallmarks of AD. Therefore, exposing neurons to various Aβ concentrations would create a disease pathology in neurons similar to AD. This will allow the characterization of *IFIT3* and *STAT1* expression regarding various Aβ concentrations. In this regard, several published data also suggested that *in vitro* AD is a unique tool to characterize the AD pathology outside *in vivo* conditions (Petry et al., 2020). In this regard, different concentration of Aβ was treated with SH-SY5Y cells to optimize a concentration that is not toxic to cells. However, that concentration also creates AD-like pathology in SH-SY5Y cells. Cell viability was observed using an MTS assay to optimize the Aβ concentration that is not toxic to cells but can induce AD-like cell pathology in SH-SY5Y cells (Figure 13). Initially, only undifferentiated SH-SY5Y cells were being measured for cell viability. This did not show any significant decrease in cell viability. A similar observation was made by other groups where cell viability was measured in undifferentiated and differentiated SH-SY5Y after exposure to Aβ (Petry et al., 2020). It was observed that differentiated SH-SY5Y were more sensitive to Aβ. This may be due to the post-mitotic characteristic, and increased receptors are seen in mature adults. This cytotoxic effect was observed in differentiated SH-SY5Y, HMC3, and HA in determining if the AD model was effective. By analyzing various cell

lines, it was observed that 60μM of Aβ was optimum for exhibiting AD-like cell pathologies within 96hrs in the SH-SY5Y cells, as indicated (Figure.13). In this regard, cell treated with 60μM of Aβ for 96 hours was optimum to observe the Aβ induced pathologies comparable to late stages of AD. Since ROS has a significant effect on AD pathology, the effect of ROS was observed on Aβ treated cells (Cheignon et al., 2018). It was observed that Aβ did not induce any ROS production in undifferentiated SH-SY5Y (Figure.14). It is possible that Aβ does not produce ROS within the time of the analysis. Our results of differentiated cells treated with 60μM of Aβ show a significant increase in ROS production compared to the other concentrations. Previous studies have reported that differentiated SH-SY5Y is more sensitive to Aβ compared to undifferentiated SH-SY5Y. They reported that undifferentiated SH-SY5Y lack neurites that reduce the surface area that Aβ can cover (Krishtal et al., 2017).

Our study has identified that *STAT1* and *IFIT3* genes are affected in AD and HAND patients in our SAM analysis. In addition, our study indicated that among other genes, *STAT1* is downregulated in the AD model, which has been associated with severe neurodegeneration. In parallel, it was also observed that *IFIT3* was also downregulated in this condition. Among the other genes, *ISG15* and *GBP1*, *IFIT3* are uncharacterized genes concerning AD pathology. Previous studies on AD brains demonstrate that severe dementia is characterized by increased downregulated genes (Haroutunian et al., 2009).

This provided an ideal opportunity to characterize this gene in this model. Therefore, the present study has characterized the *STAT1* and *IFIT3* gene in the in vitro AD model. The gene expression of *IFIT3* and *STAT1* in differentiated and undifferentiated SH-SY5Y cells through 96 hours of treatment with various Aβ concentrations (Figure 15). It was observed that there is an

upregulation of both *IFIT3* and *STAT1* at 60μM Aβ treated cells at 96 hours. This upregulation of these interferon-stimulated genes suggests that Aβ can induce the release of interferons that will recruit STAT proteins upon binding to the receptor known as the IFNAR complex on the cell membrane. When STAT proteins are recruited, they are phosphorylated and translocated to the nucleus, activating the transcription of ISGs like *IFIT3* and *ISG15*. Once the transcripts are complete, they undergo translation by rRNA to produce proteins that are the gene's functional components. However, an early study using peripheral blood samples identified a low ratio of rRNA 28S and 18S subunits in AD patients compared to age-matched and young healthy controls (Payão et al., 1998).

Our immunocytochemistry and flow cytometry significantly reduced protein expression for IFIT3 and STAT1 after 96 hours of Aβ treatment. However, results are not significant between trials. There is a reduction below the control levels in cells treated with 60μM for both differentiated and undifferentiated SH-SY5Y. Even though there is no reduction of STAT1 below control levels, there is a reduction of 60μM treated cells compared to the expression of 10μM and 20μM. Further studies should measure protein expression at different time points to fully understand gene expression's transcriptional and translation levels. A reduction in protein synthesis suggests that Aβ may be associated with the impairment of translational mechanisms that may be detrimental to the cell. Previous studies have reported impaired protein synthesis in the early stages of AD. This study suggests that impaired protein synthesis may interfere with the cell's ability to regulate hemostasis and contribute to neuronal damage (Ding et al., 2005).

Similarly, studies have shown that brain regions, specifically the frontal cortex affected by AD, have reduced mRNA translation (Langstorm et al., 1989). This supports our *in vitro*

results showing the reduced translation of *IFIT3* and *STAT1* despite the significant mRNA upregulation. A previous study that measured the protein expression in AD mice models demonstrates dysregulation of protein homeostasis (proteostasis) and pathways involved in protein degradation and synthesis before symptoms. The results suggest that reduced protein synthesis is crucial for developing AD pathology (Elder et al., 2021).

A study shows that Aβ in neurons regulates translation, affecting proteins' synthesis, and nanomolar amounts of Aβ increased translation. Their data suggest there is a biphasic regulation of translation in AD. In which earlier stages have an increased rate of translation; however, in the later stages, protein synthesis is impaired, leading to neurodegeneration (Ghosh et al., 2020). Aβ aggregates can be resistant to phagocytotic degradation; therefore, they can be found in the brains of people with AD. It is suggested that Aβ can be recognized by Toll-like Receptors as if they were pathogen-associated molecular patterns (PAMP)-like agents initiating a pro-inflammatory response (Udan et al., 2008). Previous results demonstrate that both *TLR4* and *TLR7* are upregulated in AD subjects. This observation is supported by a study that suggested the expression of *TLR4* increases with age (Hughes et al., 2020). Downstream TLR activation induces the expression of type 1 interferons that then activate the transcription of ISGs through the JAK-STAT pathway, as seen in Figure 18. In the CNS, all cells can produce type 1 interferons; however, the effects in the brain of AD are still not well characterized. It has been observed that increased levels of IFN-α are detrimental to the brain, and type 1 interferons can induce pro-apoptotic signaling in neurons. The results in Figure 16-17 from our study show a deficiency in STAT1 protein after 96 hours of Aβ treatment. Studies in mice have demonstrated that STAT1 deficiency in the CNS prevents the activation of IFN dependent genes, suggesting its

distinctive role in the CNS (Pasieka et al., 2011). Data indicate that IFN-α response in neurons depends entirely on STAT1 (Wang & Campbell, 2005). The STAT1 depletion in the neurons is compensated by activating STAT3, which contributes to pathology in the CNS (Pasieka et al., 2011). The activated STAT3 can be phosphorylated in response to IFN-ß and IFN-γ that downregulates TNF-A and NFKB (Kim et al., 2015). Our results also show downregulation of IFIT3 protein expression in SH-SY5Y cells after 96-hour incubation with Aβ. Based on our results, cells treated for 96 hours also showed a significant decrease in cell viability. Studies showed that *IFIT3* knockout increased cell death by measuring caspase3/7 levels (Sasaki et al., 2021).

Similarly, other studies have observed that silencing *IFIT3* is associated with more significant cell death in astrocytoma cells (Hsu et al., 2013). Recent studies show that IFIT3 can regulate mitochondrial apoptosis in human pancreatic cells (Wang et al., 2020). Based on our results, we can associate the reduction of *IFIT3* expression to increase levels of cell death. However, further research is needed to confirm that *IFIT3* is associated with cell death seen in SH-SY5Y.

Based on the given observation made through computational analysis with the supportive evidence of primary science data, we propose a downregulation in the gene expression of both *IFIT3* and *STAT1*. Our data suggest an impairment in these genes' translation despite an increased number of *STAT1* and *IFIT3* transcripts in differentiated SH-SY5Y cells. The inconsistent results of mRNA expression in undifferentiated SH-SY5Y may result from the heterogeneous population of cells at different stages of mitosis instead of the homogenous population seen in differentiated SH-SY5Y. Both cells types had a significant reduction in

protein expression, suggesting a reduced function of these genes at 96 hours of Aβ treatment. The gene expression for *IFIT3* and *STAT1* in the first aim of this study used total RNA to measure gene expression through GWAS. There was no protein data to compare with the *in vitro* study; however, it can be implied that a reduced number of transcripts will reduce protein synthesis. What can be observed in AD patients is an upregulation of both *TLR4* and *TLR7*, which can activate the transcription of Type 1 interferons that can signal through the JAK-STAT pathway (Figure. 18). However, the downregulation of STAT1 means that it can not be recruited to the cell membrane to activate downstream transcription of ISGs, including *IFIT3* and *ISG15*. Previous studies have shown that it increases apoptosis in cells. This study reports a reduced level of *IFIT3* expression in differentiated cells treated with 60μM of Aβ for 96 hours. These differentiated cells also showed significant cell death at 96 hours. Therefore, it is worth mentioning that future studies should investigate the correlation between cell death and reduced *IFIT3* expression in the AD model.

Nonetheless, this study did not address the expression levels of *IFIT3* and *STAT1* in HAND pathology, which can be done in future analysis (Figure. 19). However, our experimental data suggested that the population living with HIV-1 has an upregulation of genes involved in the Type 1 interferon pathway. The virus can be recognized by *TLR7* that was shown to be upregulated in the white matter of untreated HAND patients. This can activate the transcription of interferons that will signal through the JAK-STAT pathway. There was a significant upregulation of *STAT1*, suggesting that it can be recruited and phosphorylated. After forming the heterodimer, it is translocated into the nucleus, where it can activate the transcription of ISGs.

Our data showed a significant upregulation of ISGs *IFIT3* and *ISG15*. It would be worth investigating the role of *IFIT3*, specifically its role in neuroinflammation.

Our results suggest an impaired innate immune response in AD patients, specifically the Type 1 and 2 interferon pathways. This is supported by a post mortem AD brain study that reported a decrease in *IFN-α* and *IRF7*. Interestingly, the same study observed an increase of *IFN-α* and *IRF7* in the hippocampus, meaning a differential expression in distinct regions of the brain (Romagnoli et al., 2020). This may explain why we see the opposite regulation of type 1 and 2 interferon pathways in AD and HAND—unpublished data in our lab show downregulation of *IFIT3* in HAD vs. HIV frontal cortex. In the white matter of untreated HAND, there is an upregulation of *IFIT3*. It has been observed that impaired immune response varies in different brain regions; therefore, we do not rule out that there could be different expression levels in other regions of the brain. The white matter of people with AD has been suggested to be associated with cognitive impairment. It would be interesting to see the expression of genes in this part of the brain (Nasrabady et al., 2018). The white matter is a reservoir for HIV-1 infected during the early stages of the disease (Rumbaugh & Tyor, 2015). Many studies have focused on investigating brain tissue samples to identify the critical pathophysiological features of the patients with different severity levels of HAND (Rumbaugh and Tyor, 2015).

The activated microglial cells elicit an immune response releasing proinflammatory cytokines that may cause neuronal damage. Microglia may have a role in developing neurological diseases like AD and HAND (Borrajo et al., 2021). A recent study on AD post mortem brains reported dysregulation of type 1 interferons in distinct regions of the brains (Romagnoli et al., 2020). Future studies to further understand the immune response in

neurodegenerative diseases like HAND and AD should compare the same regions of the brain for more consistent results. Even though HAD is rare and no longer relevant, it shows the dysregulation of *IFIT3* in different neurodegenerative diseases and that tight regulation of *IFIT3* may be beneficial.

Conclusion

In conclusion, we accept the hypothesis due to the reduction of *STAT1* and *IFIT3* gene expression in AD *ex vivo* and *in vitro* models. However, further tests are needed to gain statistical significance for the *in vitro* model. Measuring gene expression over some time is key to understanding their regulation. Our study supports previous reports of impaired innate immunity in people with AD (Mulugeta et al., 2008). Specifically, a dysregulated type 1 interferon pathway may lead to severe neurodegeneration. Further investigation is needed to understand these genes' function in the development of AD pathology.

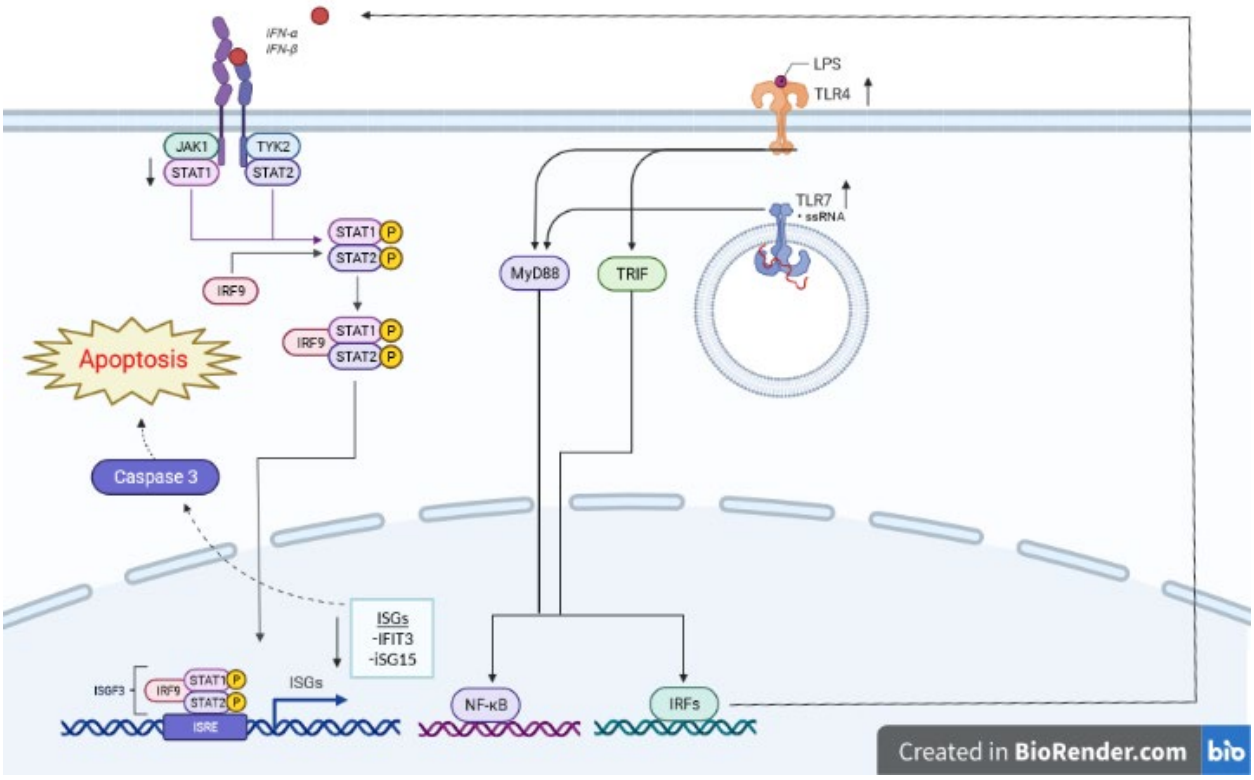

Figure 19: Proposed Type 1 Interferon in AD Pathology. Based on our data from Aim 1, we propose that in AD pathology, there is an initial upregulation in Toll-Like receptors TLR4 and TLR7, which activate the expression of Type 1 interferons. However, the data suggests that there is a downregulation of STAT1, which will inhibit the activation of downstream gene IFIT3. Previous studies have shown that cell apoptosis increases as a result of IFIT3 reduction in cells. Further research is needed to confirm this in AD.

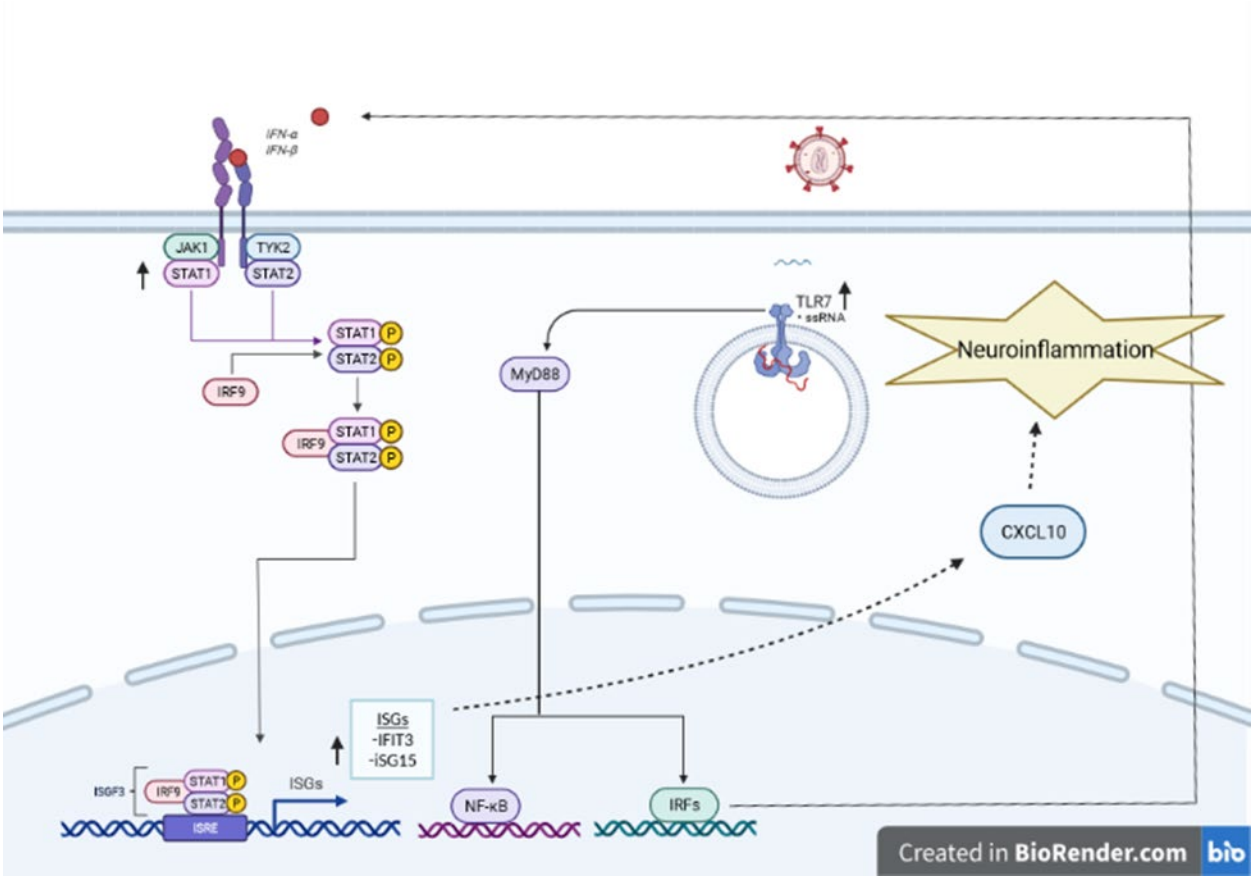

Figure 20: Proposed Type 1 Interferon in HAND Pathology. Based on our data from Aim 1, we propose that in HAND pathology, there is an initial upregulation in Toll-Like receptors TLR7 which will activate the expression of Type 1 interferons. The upregulation of STAT1 enables the protein to be recruited and activate the downstream expression of ISGs like IFIT3 and ISG15. Studies have shown the ability of IFIT3 (ISG60) to regulate chemokine CXCL10. Future research is needed to determine its potential association with chronic neuroinflammation.

REFERENCES

Achim, C.L., Adame, A., Dumaop, W., Everall, I. P., & Masliah, E. (2009). Increased Accumulation of Intraneuronal Amyloid β in HIV-Infected Patients. *Journal of Neuroimmune Pharmacology*, *4*(2), 190–199. https://doi.org/10.1007/s11481-009-9152-8

Alzheimer's Association. (2020). 2020 Alzheimer's disease facts and figures. *Alzheimer's & Dementia*, *16*(3), 391–460. https://doi.org/10.1002/alz.12068

Ayton, J. (2020). Acute phase markers in CSF reveal inflammatory changes in Alzheimer's disease that intersect with pathology, APOE ε4, sex and age. *Progress in Neurobiology*, 101904–101904.

Belkhelfa, M., Rafa, H., Medjeber, O., Arroul-Lammali, A., Behairi, N., Abada-Bendib, M., Makrelouf, M., Belarbi, S., Masmoudi, A. N., Tazir, M., & Touil-Boukoffa, C. (2014). IFN-γ and TNF-α Are Involved During Alzheimer Disease Progression and Correlate with Nitric Oxide Production: A Study in Algerian Patients. *Journal of Interferon & Cytokine Research*, *34*(11), 839–847. https://doi.org/10.1089/jir.2013.0085

Berry, B.J., Smith, A. S. T., Long, C. J., Martin, C. C., & Hickman, J. J. (2018). Physiological Aβ Concentrations Produce a More Biomimetic Representation of the Alzheimer's Disease Phenotype in iPSC Derived Human Neurons. *ACS Chemical Neuroscience*, *9*(7), 1693–1701. https://doi.org/10.1021/acschemneuro.8b00067

Bhattacharya, S., & Montag, D. (2015). Acetylcholinesterase inhibitor modifications： a promising strategy to delay the progression of Alzheimer＇s disease. *Neural Regeneration Research*, *10*(1), 43–45. https://doi.org/10.4103/1673-5374.150648

Bilousova, T., Simmons, B. J., Knapp, R. R., Elias, C. J., Campagna, J., Melnik, M., Chandra, S., Focht, S., Zhu, C., Vadivel, K., Jagodzinska, B., Cohn, W., Spilman, P., Gylys, K. H., Garg, N. K., & John, V. (2020). Dual Neutral Sphingomyelinase-2/Acetylcholinesterase Inhibitors for the Treatment of Alzheimer's Disease. *ACS Chemical Biology*, *15*(6), 1671–1684. https://doi.org/10.1021/acschembio.0c00311

Borden, E.C., Sen, G. C., Uze, G., Silverman, R. H., Ransohoff, R. M., Foster, G. R., & Stark, G. R. (2007). Interferons at age 50: past, current and future impact on biomedicine. *Nature Reviews. Drug Discovery*, *6*(12), 975–990. https://doi.org/10.1038/nrd2422

Borrajo, A., Spuch, C., Penedo, M. A., Olivares, J. M., & Agís-Balboa, R. C. (2021). Important role of microglia in HIV-1 associated neurocognitive disorders and the molecular pathways implicated in its pathogenesis. *Annals of Medicine (Helsinki)*, *53*(1), 43–69. https://doi.org/10.1080/07853890.2020.1814962

Canet, G., Chevallier, N., Zussy, C., Desrumaux, C., & Givalois, L. (2018). Central Role of Glucocorticoid Receptors in Alzheimer's Disease and Depression. *Frontiers in Neuroscience*, *12*, 739–739.

Cheignon, C., Tomas, M., Bonnefont-Rousselot, D., Faller, P., Hureau, C., & Collin, F. (2018). Oxidative stress and the amyloid beta peptide in Alzheimer's disease. *Redox Biology*, *14*, 450–464. https://doi.org/10.1016/j.redox.2017.10.014

Chu, G., Narasimham, B., Tibshirani, R. and Tusher, V. G. (2005). SAM "Significance Analysis of Microarrays" Users guide and technical document. Policy.

Clough, E., & Barrett, T. (2016). The Gene Expression Omnibus Database. Methods Mol Biol 1418, 93-110

Colovic, M. B., Krstic, D. Z., Lazarevic-Pasti, T. D., Bondzic, A. M., & Vasic, V. M. (2013). Acetylcholinesterase Inhibitors: Pharmacology and Toxicology. *Current Neuropharmacology*, *11*(3), 315–335. https://doi.org/10.2174/1570159X11311030006

Dansokho, C., Ahmed, D. A., Aid, S., Toly-Ndour, C., Chaigneau, T., Calle, V., Cagnard, N., Holzenberger, M., Piaggio, E., Aucouturier, P., & Dorothee, G. (2016). O2-07-03: Regulatory T Cells Delay Disease Progression in Alzheimer's-Like Pathology. *Alzheimer's & Dementia*, *12*(7S_Part_5), P242–P242. https://doi.org/10.1016/j.jalz.2016.06.432

DeKosky, S. T., & Scheff, S. W. (1990). Synapse loss in frontal cortex biopsies in Alzheimer's disease: correlation with cognitive severity. *Annals of neurology*, *27*(5), 457–464. https://doi.org/10.1002/ana.410270502

De Strooper, B., & Annaert, W. (2000). Proteolytic processing and cell biological functions of the amyloid precursor protein. *Journal of Cell Science*, *113 (Pt 11)*, 1857–1870.

Ding, Q., Markesbery, W. R., Chen, Q., Li, F., & Keller, J. N. (2005). Ribosome dysfunction is an early event in Alzheimer's disease. The Journal of neuroscience : the official journal of the Society for Neuroscience, 25(40), 9171–9175. https://doi.org/10.1523/JNEUROSCI.3040-05.2005

Elder, M. K., Erdjument-Bromage, H., Oliveira, M. M., Mamcarz, M., Neubert, T. A., & Klann, E. (2021). Age-dependent shift in the de novo proteome accompanies pathogenesis in an Alzheimer's disease mouse model. Communications Biology, 4(1), 823. https://doi.org/10.1038/s42003-021-02324-6

Esiri, M. M., Biddolph, S. C., & Morris, C. S. (1998). Prevalence of Alzheimer plaques in AIDS. Journal of Neurology, Neurosurgery & Psychiatry, 65(1), 29–33. https://doi.org/10.1136/jnnp.65.1.29

Everall, I., Salaria, S., Roberts, E., Corbeil, J., Sasik, R., Fox, H., Grant, I., & Masliah, E. (2005). Methamphetamine stimulates interferon inducible genes in HIV infected brain. *Journal of Neuroimmunology*, *170*(1), 158–171. https://doi.org/10.1016/j.jneuroim.2005.09.009

Fang, F., & Liu, G. (2008). Novel squamosamide derivative (compound FLZ) attenuates Aβ25–35-induced toxicity in SH-SY5Y cells. *Acta Pharmacologica Sinica*, *29*(2), 152–160. https://doi.org/10.1111/j.1745-7254.2008.00714.x

Fensterl, V., & Sen, G. C. (2015). Interferon-induced Ifit proteins: their role in viral pathogenesis. *Journal of Virology*, *89*(5), 2462–2468. https://doi.org/10.1128/JVI.02744-14

Ferreira-Vieira, T.H., Guimaraes, I. M., Silva, F. R., & Ribeiro, F. M. (2016). Alzheimer's disease: Targeting the Cholinergic System. *Current Neuropharmacology*, *14*(1), 101–115. https://doi.org/10.2174/1570159X13666150716165726

Fields, J., Dumaop, W., Adame, A., Ellis, R. J., Letendre, S., Grant, I., & Masliah, E. (2013). Alterations in the Levels of Vesicular Trafficking Proteins Involved in HIV Replication in the Brains and CSF of Patients with HIV-associated Neurocognitive Disorders. *Journal of Neuroimmune Pharmacology*, *8*(5), 1197–1209. https://doi.org/10.1007/s11481-013-9511-3

Fields, J., Spencer, B., Swinton, M., Qvale, E. M., Marquine, M. J., Alexeeva, A., Gough, S., Soontornniyomkij, B., Valera, E., Masliah, E., Achim, C. L., & Desplats, P. (2018). Alterations in brain TREM2 and Amyloid-β levels are associated with neurocognitive impairment in HIV-infected persons on antiretroviral therapy. *Journal of Neurochemistry*, *147*(6), 784–802. https://doi.org/10.1111/jnc.14582

Fields, J., Swinton, M. K., Soontornniyomkij, B., Carson, A., & Achim, C. L. (2020). Beta amyloid levels in cerebrospinal fluid of HIV-infected people vary by exposure to antiretroviral therapy. *AIDS (London)*, *34*(7), 1001–1007. https://doi.org/10.1097/QAD.0000000000002506

Fulop, T., Witkowski, J. M., Larbi, A., Khalil, A., Herbein, G., & Frost, E. H. (2019). Does HIV infection contribute to increased beta-amyloid synthesis and plaque formation leading to neurodegeneration and Alzheimer's disease? *Journal of Neurovirology*, *25*(5), 634–647. https://doi.org/10.1007/s13365-019-00732-3

Garcia-Mesa, Y., Jay, T. R., Checkley, M. A., Luttge, B., Dobrowolski, C., Valadkhan, S., Landreth, G. E., Karn, J., & Alvarez-Carbonell, D. (2016). Immortalization of primary microglia: a new platform to study HIV regulation in the central nervous system. *Journal of Neurovirology*, *23*(1), 47–66. https://doi.org/10.1007/s13365-016-0499-3

Gelman, B., Chen, T., Lisinicchia, J. G., Soukup, V. M., Carmical, J. R., Starkey, J. M., Masliah, E., Commins, D. L., Brandt, D., Grant, I., Singer, E. J., Levine, A. J., Miller, J., Winkler, J. M., Fox, H. S., Luxon, B. A., & Morgello, S. (2012). The National NeuroAIDS Tissue Consortium brain gene array: two types of HIV-associated neurocognitive impairment. *PloS One*, *7*(9), e46178–e46178. https://doi.org/10.1371/journal.pone.0046178

Ghosh, A., Mizuno, K., Tiwari, S. S., Proitsi, P., Gomez Perez-Nievas, B., Glennon, E., Martinez-Nunez, R. T., & Giese, K. P. (2020). Alzheimer's disease-related dysregulation of mRNA translation causes key pathological features with ageing. Translational psychiatry, 10(1), 192. https://doi.org/10.1038/s41398-020-00882-7

Gómez, C., Perdiguero, B., Falqui, M., Marín, M. Q., Bécares, M., Sorzano, C. Ó. S., García-Arriaza, J., Esteban, M., & Guerra, S. (2020). Enhancement of HIV-1 Env-Specific CD8 T Cell Responses Using Interferon-Stimulated Gene 15 as an Immune Adjuvant. *Journal of Virology*, *95*(2). https://doi.org/10.1128/JVI.01155-20

Green, D.A., Masliah, E., Vinters, H. V., Beizai, P., Moore, D. J., & Achim, C. L. (2005). Brain deposition of beta-amyloid is a common pathologic feature in HIV positive patients. AIDS (London), 19(4), 407–411. https://doi.org/10.1097/01.aids.0000161770.06158.5c

Hariri, S., & Mckenna, M. T. (2007). Epidemiology of Human Immunodeficiency Virus in the United States. *Clinical Microbiology Reviews*, *20*(3), 478–488. https://doi.org/10.1128/CMR.00006-07

Haroutunian, V., Katsel, P., & Schmeidler, J. (2009). Transcriptional vulnerability of brain regions in Alzheimer's disease and dementia. Neurobiology of Aging, 30(4), 561–573. https://doi.org/10.1016/j.neurobiolaging.2007.07.021

Hashimoto, M., Katakura, M., Hossain, S., Rahman, A., Shimada, T., & Shido, O. (2011). Docosahexaenoic acid withstands the Aβ(25-35)-induced neurotoxicity in SH-SY5Y cells. *The Journal of Nutritional Biochemistry*, *22*(1), 22–.

Hippius, H., & Neundörfer, G. (2003). The discovery of Alzheimer's disease. *Dialogues in Clinical Neuroscience*, *5*(1), 101–108. https://doi.org/10.31887/DCNS.2003.5.1/hhippius

Howdle, G., Quidé, Y., Kassem, M. S., Johnson, K., Rae, C. D., Brew, B. J., & Cysique, L. A. (2020). Brain amyloid in virally suppressed HIV-associated neurocognitive disorder. *Neurology : Neuroimmunology & Neuroinflammation*, *7*(4), e739–e739. https://doi.org/10.1212/NXI.0000000000000739

Hsu, W., Ma, Y.-L., Hsieh, D.-Y., Liu, Y.-C., & Lee, E. H. (2014). STAT1 negatively regulates spatial memory formation and mediates the memory-impairing effect of Aβ. *Neuropsychopharmacology (New York, N.Y.)*, *39*(3), 746–758. https://doi.org/10.1038/npp.2013.263

Hsu, Y. L., Shi, S.-F., Wu, W.-L., Ho, L.-J., & Lai, J.-H. (2013). Protective roles of interferon-induced protein with tetratricopeptide repeats 3 (IFIT3) in dengue virus infection of human lung epithelial cells. PloS One, 8(11), e79518–e79518. https://doi.org/10.1371/journal.pone.0079518

Huang, D.W., Lempicki, R. A., & Sherman, B. T. (2008). Systematic and integrative analysis of large gene lists using DAVID bioinformatics resources. *Nature Protocols*, *4*(1), 44–57. https://doi.org/10.1038/nprot.2008.211

Hughes, C.,Choi, M. L., Yi, J.-H., Kim, S.-C., Drews, A., George-Hyslop, P. S., Bryant, C., Gandhi, S., Cho, K., & Klenerman, D. (2020). Beta amyloid aggregates induce sensitised TLR4 signalling causing long-term potentiation deficit and rat neuronal cell death. *Communications Biology*, *3*(1), 79–79. https://doi.org/10.1038/s42003-020-0792-9

Hwang, M., & Bergmann, C. C. (2020). Neuronal Ablation of Alpha/Beta Interferon (IFN-α/β) Signaling Exacerbates Central Nervous System Viral Dissemination and Impairs IFN-γ

Responsiveness in Microglia/Macrophages. *Journal of Virology*, *94*(20). https://doi.org/10.1128/JVI.00422-20

Imaizumi, T., Yoshida, H., Hayakari, R., Xing, F., Wang, L., Matsumiya, T., Tanji, K., Kawaguchi, S., Murakami, M., & Tanaka, H. (2016). Interferon-stimulated gene (ISG) 60, as well as ISG56 and ISG54, positively regulates TLR3/IFN-β/STAT1 axis in U373MG human astrocytoma cells. Neuroscience Research, 105, 35–41. https://doi.org/10.1016/j.neures.2015.09.002

Isik, A.T. (2010). Late onset Alzheimer's disease in older people. *Clinical Interventions in Aging*, *5*, 307–311. https://doi.org/10.2147/CIA.S11718

Jefferson, A.L., Gibbons, L. E., Rentz, D. M., Carvalho, J. O., Manly, J., Bennett, D. A., & Jones, R. N. (2011). A Life Course Model of Cognitive Activities, Socioeconomic Status, Education, Reading Ability, and Cognition. Journal of the American Geriatrics Society (JAGS), 59(8), 1403–1411. https://doi.org/10.1111/j.1532-5415.2011.03499.x

Jin, Z., Zhang, C., Liu, M., Jiao, S., Zhao, J., Liu, X., Lin, H., Chi-cheong Wan, D., & Hu, C. (2021). Synthesis, biological activity, molecular docking studies of a novel series of 3-Aryl-7H-thiazolo[3,2-b]-1,2,4-triazin-7-one derivatives as the acetylcholinesterase inhibitors. *Journal of Biomolecular Structure & Dynamics*, *39*(7), 2478–2489. https://doi.org/10.1080/07391102.2020.1753576

Khan, N., Haughey, N. J., Nath, A., & Geiger, J. D. (2019). Involvement of organelles and inter-organellar signaling in the pathogenesis of HIV-1 associated neurocognitive disorder and Alzheimer's disease. *Brain Research*, *1722*, 146389–146389. https://doi.org/10.1016/j.brainres.2019.146389

Kim, H.S., Kim, D. C., Kim, H.-M., Kwon, H.-J., Kwon, S. J., Kang, S.-J., Kim, S. C., & Choi, G.-E. (2015). STAT1 deficiency redirects IFN signalling toward suppression of TLR response through a feedback activation of STAT3. Scientific Reports, 5(1), 13414–13414. https://doi.org/10.1038/srep13414

Kodidela, S., Gerth, K., Haque, S., Gong, Y., Ismael, S., Singh, A., Tauheed, I., & Kumar, S. (2019). Extracellular Vesicles: A Possible Link between HIV and Alzheimer's Disease-Like Pathology in HIV Subjects? *Cells (Basel, Switzerland)*, *8*(9), 968–. https://doi.org/10.3390/cells8090968

Krishtal, J., Bragina, O., Metsla, K., Palumaa, P., & Tõugu, V. (2017). In situ fibrillizing amyloid-beta 1-42 induces neurite degeneration and apoptosis of differentiated SH-SY5Y cells. *PloS One*, *12*(10), e0186636–. https://doi.org/10.1371/journal.pone.0186636

Kuffour, E.O., König, R., Häussinger, D., Schulz, W. A., & Münk, C. (2019). ISG15 Deficiency Enhances HIV-1 Infection by Accumulating Misfolded p53. *mBio*, *10*(4), e01342–19–. https://doi.org/10.1128/mBio.01342-19

Langstrom, N.S., Anderson, J. ., Lindroos, H. ., Winbland, B., & Wallace, W. . (1989). Alzheimer's disease-associated reduction of polysomal mRNA translation. *Brain Research. Molecular Brain Research.*, *5*(4), 259–269. https://doi.org/10.1016/0169-328X(89)90060-0

Lattanzio, F., Carboni, L., Carretta, D., Candeletti, S., & Romualdi, P. (2016). Treatment with the neurotoxic Aβ (25-35) peptide modulates the expression of neuroprotective factors Pin1, Sirtuin 1, and brain-derived neurotrophic factor in SH-SY5Y human neuroblastoma cells. *Experimental and toxicologic pathology : official journal of the Gesellschaft fur Toxikologische Pathologie*, *68*(5), 271–276.

Lee, E., Chanamara, S., Pleasure, D., & Soulika, A. M. (2012). IFN-gamma signaling in the central nervous system controls the course of experimental autoimmune encephalomyelitis independently of the localization and composition of inflammatory foci. *Journal of Neuroinflammation*, *9*(1), 7–7. https://doi.org/10.1186/1742-2094-9-7

Li, L., Liu, M., Jiang, X., Xia, Z., Wang, Y., An, D., Wang, H., Heng, B., & Liu, Y. (2019). Metformin inhibits Aβ25-35-induced apoptotic cell death in SH-SY5Y cells. *Basic & Clinical Pharmacology & Toxicology*, *125*(5), 439–449. https://doi.org/10.1111/bcpt.13279

Liang, W., Dunckley, T., Beach, T. G., Grover, A., Mastroeni, D., Ramsey, K., Caselli, R. J., Kukull, W. A., McKeel, D., Morris, J. C., Hulette, C. M., Schmechel, D., Reiman, E. M., Rogers, J., & Stephan, D. A. (2008). Altered neuronal gene expression in brain regions differentially affected by Alzheimer's disease: a reference data set. *Physiological Genomics*, *33*(2), 240–256. https://doi.org/10.1152/physiolgenomics.00242.2007

Litvinchuk, A., Wan, Y.-W., Swartzlander, D. B., Chen, F., Cole, A., Propson, N. E., Wang, Q., Zhang, B., Liu, Z., & Zheng, H. (2018). Complement C3aR Inactivation Attenuates Tau Pathology and Reverses an Immune Network Deregulated in Tauopathy Models and Alzheimer's Disease. *Neuron (Cambridge, Mass.)*, *100*(6), 1337–1353.e5. https://doi.org/10.1016/j.neuron.2018.10.031

Liu, S., Ma, Y., Hsu, W., Chiou, H., & Lee, E. H. . (2019). Protein inhibitor of activated STAT1 Ser503 phosphorylation-mediated Elk-1 SUMOylation promotes neuronal survival in APP/PS1 mice. *British Journal of Pharmacology*, *176*(11), 1793–1810. https://doi.org/10.1111/bph.14656

Malakhova, O., Malakhov, M., Hetherington, C., & Zhang, D.-E. (2002). Lipopolysaccharide Activates the Expression of ISG15-specific Protease UBP43 via Interferon Regulatory Factor 3. *The Journal of Biological Chemistry*, *277*(17), 14703–14711. https://doi.org/10.1074/jbc.M111527200

Masliah, E., Roberts, E. S., Langford, D., Everall, I., Crews, L., Adame, A., Rockenstein, E., & Fox, H. S. (2004). Patterns of gene dysregulation in the frontal cortex of patients with HIV encephalitis. *Journal of Neuroimmunology*, *157*(1), 163–175. https://doi.org/10.1016/j.jneuroim.2004.08.026

Meier, A., Alter, G., Frahm, N., Sidhu, H., Li, B., Bagchi, A., Teigen, N., Streeck, H., Stellbrink, H.-J., Hellman, J., van Lunzen, J., & Altfeld, M. (2007). MyD88-Dependent Immune Activation Mediated by Human Immunodeficiency Virus Type 1-Encoded Toll-Like Receptor Ligands. *Journal of Virology*, *81*(15), 8180–8191. https://doi.org/10.1128/JVI.00421-07

Milanini, B., Samboju, V., Cobigo, Y., Paul, R., Javandel, S., Hellmuth, J., Allen, I., Miller, B., & Valcour, V. (2019). Longitudinal brain atrophy patterns and neuropsychological performance in older adults with HIV-associated neurocognitive disorder compared with early Alzheimer's disease. *Neurobiology of Aging*, *82*, 69–76. https://doi.org/10.1016/j.neurobiolaging.2019.07.006

Mulugeta, E., Molina-Holgado, F., Elliott, M. S., Hortobagyi, T., Perry, R., Kalaria, R. N., Ballard, C. G., & Francis, P. T. (2008). Inflammatory mediators in the frontal lobe of patients with mixed and vascular dementia. *Dementia and geriatric cognitive disorders*, *25*(3), 278–286. https://doi.org/10.1159/000118633

Nasrabady, S.E., Rizvi, B., Goldman, J. E., & Brickman, A. M. (2018). White matter changes in Alzheimer's disease: a focus on myelin and oligodendrocytes. Acta Neuropathologica Communications, 6(1), 22–10. https://doi.org/10.1186/s40478-018-0515-3

Nativio, R., Donahue, G., Berson, A., Lan, Y., Amlie-Wolf, A., Tuzer, F., Toledo, J. B., Gosai, S. J., Gregory, B. D., Torres, C., Trojanowski, J. Q., Wang, L.-S., Johnson, F. B., Bonini, N. M., & Berger, S. L. (2018). Dysregulation of the epigenetic landscape of normal aging in Alzheimer's disease. *Nature Neuroscience*, *21*(4), 497–505. https://doi.org/10.1038/s41593-018-0101-9

Nazarian, A., Arbeev, K. G., Yashkin, A. P., & Kulminski, A. M. (2019). Genetic heterogeneity of Alzheimer's disease in subjects with and without hypertension. *GeroScience*, *41*(2), 137–154. https://doi.org/10.1007/s11357-019-00071-5

Nitkiewicz, J., Borjabad, A., Morgello, S., Murray, J., Chao, W., Emdad, L., Fisher, P. B., Potash, M. J., & Volsky, D. J. (2017). HIV induces expression of complement component C3 in astrocytes by NF-κB-dependent activation of interleukin-6 synthesis. *Journal of Neuroinflammation*, *14*(1), 23–23. https://doi.org/10.1186/s12974-017-0794-9

Okello, E.J., & Mather, J. (2020). Comparative Kinetics of Acetyl- and Butyryl-Cholinesterase Inhibition by Green Tea Catechins: Relevance to the Symptomatic Treatment of Alzheimer's Disease. *Nutrients*, *12*(4), 1090–. https://doi.org/10.3390/nu12041090

Pasieka, T. J., Cilloniz, C., Carter, V. S., Rosato, P., Katze, M. G., & Leib, D. A. (2011). Functional genomics reveals an essential and specific role for Stat1 in protection of the central nervous system following herpes simplex virus corneal infection. *Journal of virology*, *85*(24), 12972–12981. https://doi.org/10.1128/JVI.06032-11

Payão, S.L.M., Smith, M. de A. C., Winter, L. M. F., & Bertolucci, P. H. F. (1998). Ribosomal RNA in Alzheimer's disease and ageing. *Mechanisms of Ageing and Development*, *105*(3), 265–272. https://doi.org/10.1016/S0047-6374(98)00095-5

Petry, V.K., Coelho, B. P., Gaelzer, M. M., Kreutz, F., Guma, F. T. C. R., Salbego, C. G., & Trindade, V. M. T. (2020). Genistein protects against amyloid-beta-induced toxicity in SH-SY5Y cells by regulation of Akt and Tau phosphorylation. *Phytotherapy Research*, *34*(4), 796–807. https://doi.org/10.1002/ptr.6560

Pidugu, V., Pidugu, H. B., Wu, M.-M., Liu, C.-J., & Lee, T.-C. (2019). Emerging Functions of Human IFIT Proteins in Cancer. *Frontiers in Molecular Biosciences*, *6*, 148–148. https://doi.org/10.3389/fmolb.2019.00148

Platanias, L.C. (2005). Mechanisms of type-I- and type-II-interferon-mediated signalling. *Nature Reviews. Immunology*, *5*(5), 375–386. https://doi.org/10.1038/nri1604 Pulliam, L., Sun, B., Mustapic, M., Chawla, S., & Kapogiannis, D. (2019). Plasma neuronal exosomes serve as biomarkers of cognitive impairment in HIV infection and Alzheimer's disease. *Journal of Neurovirology*, *25*(5), 702–709.

Pulliam, L., Sun, B., Mustapic, M., Chawla, S., & Kapogiannis, D. (2019). Plasma neuronal exosomes serve as biomarkers of cognitive impairment in HIV infection and Alzheimer's disease. *Journal of Neurovirology*, *25*(5), 702–709. https://doi.org/10.1007/s13365-018-0695-4

Riphagen, J.M., Ramakers, I. H. G. ., Freeze, W. M., Pagen, L. H. ., Hanseeuw, B. J., Verbeek, M. M., Verhey, F. R. ., & Jacobs, H. I. . (2020). Linking APOE-ε4, blood-brain barrier dysfunction, and inflammation to Alzheimer's pathology. *Neurobiology of Aging*, *85*, 96–103. https://doi.org/10.1016/j.neurobiolaging.2019.09.020

Rosenthal, J., & Tyor, W. (2019). Aging, comorbidities, and the importance of finding biomarkers for HIV-associated neurocognitive disorders. *Journal of Neurovirology*, *25*(5), 673–685. https://doi.org/10.1007/s13365-019-00735-0

Romagnoli, M., Porcellini, E., Carbone, I., Veerhuis, R., & Licastro, F. (2020). Impaired innate immunity mechanisms in the brain of Alzheimer's disease. *International Journal of Molecular Sciences*, *21*(3), 1126–. https://doi.org/10.3390/ijms21031126

Roshan, R., Choudhary, A., Bhambri, A., Bakshi, B., Ghosh, T., & Pillai, B. (2017). microRNA dysregulation in polyglutamine toxicity of TATA-box binding protein is mediated through STAT1 in mouse neuronal cells. *Journal of Neuroinflammation*, *14*(1), 155–155. https://doi.org/10.1186/s12974-017-0925-3

Roy, E., Wang, B., Wan, Y.-W., Chiu, G., Cole, A., Yin, Z., Propson, N. E., Xu, Y., Jankowsky, J. L., Liu, Z., Lee, V. M.-Y., Trojanowski, J. Q., Ginsberg, S. D., Butovsky, O., Zheng, H., & Cao, W. (2020). Type I interferon response drives neuroinflammation and synapse loss in Alzheimer disease. *The Journal of Clinical Investigation*, *130*(4), 1912–1930. https://doi.org/10.1172/JCI133737

Rubin, L., Sundermann, E. E., & Moore, D. J. (2019). The current understanding of overlap between characteristics of HIV-associated neurocognitive disorders and Alzheimer's disease. *Journal of Neurovirology*, *25*(5), 661–672. https://doi.org/10.1007/s13365-018-0702-9

Rumbaugh, J., & Tyor, W. (2015). HIV-associated neurocognitive disorders: Five new things. *Neurology. Clinical Practice*, *5*(3), 224–231. https://doi.org/10.1212/CPJ.0000000000000117

Sasaki, M., Sato, Y., & Nakanuma, Y. (2021). Interferon-induced protein with tetratricopeptide repeats 3 may be a key factor in primary biliary cholangitis. *Scientific Reports*, *11*(1), 11413–11413. https://doi.org/10.1038/s41598-021-91016-6

Sattler, C., Toro, P., Schönknecht, P., & Schröder, J. (2012). Cognitive activity, education and socioeconomic status as preventive factors for mild cognitive impairment and

Alzheimer's disease. *Psychiatry Research*, *196*(1), 90–95. https://doi.org/10.1016/j.psychres.2011.11.012

Schmittgen, T.D., & Livak, K. J. (2008). Analyzing real-time PCR data by the comparative C T method. *Nature Protocols*, *3*(6), 1101–1108. https://doi.org/10.1038/nprot.2008.73

Sengoku, R. (2020). Aging and Alzheimer's disease pathology. *Neuropathology*, *40*(1), 22–29. https://doi.org/10.1111/neup.12626

Sheffield, K.M., & Peek, M. K. (2009). Neighborhood Context and Cognitive Decline in Older Mexican Americans: Results From the Hispanic Established Populations for Epidemiologic Studies of the Elderly. *American Journal of Epidemiology*, *169*(9), 1092–1101. https://doi.org/10.1093/aje/kwp005

Smyth, G. K. (2004).Linear models and empirical bayes methods for assessing differential expression in microarray experiments. *Statistical applications in genetics and molecular biology,* 3(3),

Soontornniyomkij, V., Moore, D. J., Gouaux, B., Soontornniyomkij, B., Sinsheimer, J. S., & Levine, A. J. (2019). Associations of regional amyloid-β plaque and phospho-tau pathology with biological factors and neuropsychological functioning among HIV-infected adults. *Journal of Neurovirology*, *25*(6), 741–753. https://doi.org/10.1007/s13365-019-00761-y

Solomon, B., Koppel, R., Frankel, D., & Hanan-Aharon, E. (1997). Disaggregation of Alzheimer β -Amyloid by Site-Directed mAb. *Proceedings of the National Academy of Sciences - PNAS*, *94*(8), 4109–4112.

Solomon, I., De Girolami, U., Chettimada, S., Misra, V., Singer, E. J., & Gabuzda, D. (2017). Brain and liver pathology, amyloid deposition, and interferon responses among older HIV-positive patients in the late HAART era. *BMC Infectious Diseases*, *17*(1), 151–151. https://doi.org/10.1186/s12879-017-2246-7

Stern, A. L., Ghura, S., Gannon, P. J., Akay-Espinoza, C., Phan, J. M., Yee, A. C., Vassar, R., Gelman, B. B., Kolson, D. L., & Jordan-Sciutto, K. L. (2018). BACE1 Mediates HIV-Associated and Excitotoxic Neuronal Damage Through an APP-Dependent Mechanism. *The Journal of neuroscience : the official journal of the Society for Neuroscience*, *38*(18), 4288–4300.

Sun, L., Yang, S., Sun, H., Li, W., & Duan, S. (2019). Molecular differences in Alzheimer's disease between male and female patients determined by integrative network analysis. *Journal of Cellular and Molecular Medicine*, *23*(1), 47–58. https://doi.org/10.1111/jcmm.13852

Taylor, J.M., Minter, M. R., Newman, A. G., Zhang, M., Adlard, P. A., & Crack, P. J. (2014). Type-1 interferon signaling mediates neuro-inflammatory events in models of Alzheimer's disease. *Neurobiology of Aging*, *35*(5), 1012–1023. https://doi.org/10.1016/j.neurobiolaging.2013.10.089

Tusher, V.G., Tibshirani, R., & Chu, G. (2001). Significance Analysis of Microarrays Applied to the Ionizing Radiation Response. *Proceedings of the National Academy of Sciences - PNAS*, *98*(9), 5116–5121. https://doi.org/10.1073/pnas.091062498

Udan, M.L.D., Ajit, D., Crouse, N. R., & Nichols, M. R. (2008). Toll-like receptors 2 and 4 mediate Abeta(1-42) activation of the innate immune response in a human monocytic cell line. *Journal of Neurochemistry*, *104*(2), 524–.

UNAIDS. (2021). Fact Sheet- World AIDS Day 2021 [PDF]. https://www.unaids.org /sites/default/files/media_asset/UNAIDS_FactSheet _en.pdf.

Unger, M., Li, E., Scharnagl, L., Poupardin, R., Altendorfer, B., Mrowetz, H., Hutter-Paier, B., Weiger, T. ., Heneka, M. ., Attems, J., & Aigner, L. (2020). CD8+ T-cells infiltrate Alzheimer's disease brains and regulate neuronal- and synapse-related gene expression in APP-PS1 transgenic mice. *Brain, Behavior, and Immunity*, *89*, 67–86. https://doi.org/10.1016/j.bbi.2020.05.070

Valencia, L. (2019). Demographic Characteristics, Trends, and Projections for Texas and the Rio Grande Valley. https://demographics.texas.gov /Resources /Presentations /OSD/2019/2019_02_22_UTRGVLegislativeInterns.pdf

Vega, I. E., Cabrera, L. Y., Wygant, C. M., Velez-Ortiz, D., & Counts, S. E. (2017). Alzheimer's Disease in the Latino Community: Intersection of Genetics and Social Determinants of Health. *Journal of Alzheimer's disease : JAD*, *58*(4), 979–992.

Wang, J., & Campbell, I. L. (2005). Innate STAT1-Dependent Genomic Response of Neurons to the Antiviral Cytokine Alpha Interferon. *Journal of Virology*, *79*(13), 8295–8302. https://doi.org/10.1128/JVI.79.13.8295-8302.2005

Wang, J., Schreiber, R. D., & Campbell, I. L. (2002). STAT1 Deficiency Unexpectedly and Markedly Exacerbates the Pathophysiological Actions of IFN-α in the Central Nervous System. *Proceedings of the National Academy of Sciences - PNAS*, *99*(25), 16209–16214. https://doi.org/10.1073/pnas.252454799

Wang, L., Jin, G., Yu, H., Li, Q., & Yang, H. (2019). Protective effect of Tenuifolin against Alzheimer's disease. Neuroscience Letters, 705, 195–201. https://doi.org/10.1016/j.neulet.2019.04.045

Wang, Z., Qin, J., Zhao, J., Li, J., Li, D., Popp, M., Popp, F., Alakus, H., Kong, B., Dong, Q., Nelson, P. J., Zhao, Y., & Bruns, C. J. (2020). Inflammatory IFIT3 renders chemotherapy resistance by regulating post-translational modification of VDAC2 in pancreatic cancer. *Theranostics*, *10*(16), 7178–7192. https://doi.org/10.7150/thno.43093

Winkler, J.M., Chaudhuri, A. D., & Fox, H. S. (2012). Translating the Brain Transcriptome in NeuroAIDS: From Non-human Primates to Humans. *Journal of Neuroimmune Pharmacology*, *7*(2), 372–379. https://doi.org/10.1007/s11481-012-9344-5

Wu, Z., and Irizarry, R. (2021). Description of gcrma package. Bioconductor.

Wu, Z., Irizarry, R., Gentleman, R., Martinez-Murillo, F., & Spencer, F. (2004). A Model-Based Background Adjustment for Oligonucleotide Expression Arrays. *Journal of the American Statistical Association*, *99*(468), 909–917.

Yoon, S.Y., & Kim, D.-H. (2016). Alzheimer's disease genes and autophagy. *Brain Research*, *1649*(Pt B), 201–209. https://doi.org/10.1016/j.brainres.2016.03.018

Yu, H., Yao, L., Zhou, H., Qu, S., Zeng, X., Zhou, D., Zhou, Y., Li, X., & Liu, Z. (2014). Neuroprotection against Aβ25–35-induced apoptosis by Salvia miltiorrhiza extract in SH-SY5Y cells. *Neurochemistry International*, *75*, 89–95. https://doi.org/10.1016/j.neuint.2014.06.001

Zhang, C., Zhao, X., Lin, S., Liu, F., Ma, J., Han, Z., Jia, F., Xie, W., Zhang, Q., & Li, X. (2019). Neuroprotective Effect of ent -Kaur-15-en-17-al-18-oic Acid on Amyloid Beta Peptide-Induced Oxidative Apoptosis in Alzheimer's Disease. *Molecules (Basel, Switzerland)*, *25*(1), 142–. https://doi.org/10.3390/molecules25010142

Zhang, X., Bogunovic, D., Payelle-Brogard, B., Francois-Newton, V., Speer, S. D., Yuan, C., Volpi, S., Li, Z., Sanal, O., Mansouri, D., Tezcan, I., Rice, G. I., Chen, C., Mansouri, N., Mahdaviani, S. A., Itan, Y., Boisson, B., Okada, S., Zeng, L., Pellegrini, S. (2015). Human intracellular ISG15 prevents interferon-α/β over-amplification and auto-inflammation. *Nature (London)*, *517*(7532), 89–93. https://doi.org/10.1038/nature13801

Zhang, Z., Li, X.-G., Wang, Z.-H., Song, M., Yu, S. P., Kang, S. S., Liu, X., Zhang, Z., Xie, M., Liu, G.-P., Wang, J.-Z., & Ye, K. (2021). δ-Secretase-clFeaved Tau stimulates Aβ production via upregulating STAT1-BACE1 signaling in Alzheimer's disease. *Molecular Psychiatry*, *26*(2), 586–603. https://doi.org/10.1038/s41380-018-0286-z

Zhao, L., Huang, Y., & Zheng, J. (2013). STAT1 regulates human glutaminase 1 promoter activity through multiple binding sites in HIV-1 infected macrophages. *PloS One*, *8*(9), e76581–. https://doi.org/10.1371/journal.pone.0076581

BIOGRAPHICAL SKETCH

This thesis is completed by Armando Garces III who attended the University of Texas Rio Grande Valley in which the requirements to receive a Bachelor of Science in Biology were met in the Spring of 2019. In the Fall of 2021, the requirements for a Master of Science in Biochemistry and Molecular Biology were met. Previous professional work include employment at Texas Plant and Soil Laboratory located in Edinburg, Texas from 2017 -2019. Also, in the year 2021 the role of Graduate Research Assistant for the Department of Health and Biomedical Sciences was held. Email: mandogarces92@gmail.com